Proteolysis-targeting vaccines (PROTAVs) for robust tumor combination immunotherapy

Qiyan Wang[1,#], Ting Su[2,3,#], Furong Cheng[2,4,#], Shurong Zhou[1], Xiang Liu[1], Mi Wang[5,6], Ri Tang[1], You Xu[1], Shimiao Liao[1], Jordan Dailey[1], Guolan Xiao[1], Hanning Wen[1], Weijia Zheng[1,5], Bo Wen[1,5], Katarzyna M Tyc[7], Venkatesha Basrur[8], Jinze Liu[7], Duxin Sun[1,5], Shaomeng Wang[5,6,9], Guizhi Zhu[1,5,10] *

[1] Department of Pharmaceutical Sciences, College of Pharmacy, University of Michigan, Ann Arbor, MI 48109, USA

[2] Department of Pharmaceutics and Center for Pharmaceutical Engineering, College of Pharmacy, Virginia Commonwealth University, Richmond, VA 23298, USA

[3] State Key Laboratory for Modification of Chemical Fibers and Polymer Materials, College of Biological Science and Medical Engineering, Donghua University, Shanghai, 201620, China

[4] School of Life Sciences, Shanghai University, Shanghai, 200444, China

[5] Rogel Cancer Center, University of Michigan, Ann Arbor, MI 48109, USA

[6] Department of Internal Medicine, University of Michigan, Ann Arbor, MI 48109, USA

[7] Department of Biostatistics, School of Public Health; Bioinformatics Shared Resource, Massey Comprehensive Cancer Center; Virginia Commonwealth University, Richmond, VA 23298, USA

[8] Proteomics Resource Facility, University of Michigan, Ann Arbor, MI 48109, USA

[9] Department of Pharmacology, University of Michigan, Ann Arbor, MI 48109, USA; Department of Medicinal Chemistry, University of Michigan, Ann Arbor, MI 48109, USA

[10] Bioinnovations in Brain Cancer, Biointerfaces Institute; Center for RNA Biomedicine. University of Michigan, Ann Arbor, MI 48109, USA

[#] Equal contribution

* Corresponding author (email: guizhiz@med.umich.edu)

Abstract

Protein/peptide vaccines can improve the tumor therapeutic efficacy of immune checkpoint blockade (ICB). However, current protein/peptide vaccines elicit limited T cell responses pivotal for tumor immunotherapy. Here, we present proteolysis-targeting vaccines (PROTAVs) that facilitate antigen proteolytic processing and cross-presentation to potentiate T cell responses for robust ICB combination immunotherapy of tumors. PROTAVs are modular conjugates of protein/peptide antigens, E3 ligase-binding ligands, and linkers. In antigen-presenting cells (APCs), PROTAVs bind to E3 ligases to rapidly ubiquitinate PROTAV antigens, thereby facilitating antigen proteolytic processing by proteasome and promoting antigen cross-presentation to T cells. In mice, when co-delivered with bi-adjuvants activating cyclic-GMP-AMP synthase (cGAS) and Toll-like receptor 9 (TLR9) using lipid nanoparticles (LNPs), PROTAVs promoted the quantity and quality of $CD8^+$ T cells against antigens of proteins, synthetic long peptides, and multivalent fusion peptides. Combining PROTAVs and ICB remodels tumor immune microenvironment, promotes the complete regression rates of murine melanoma and human papillomavirus (HPV)-associated tumors, and eradicates 50% ICB-resistant large tumors (300 mm^3). Overall, PROTAVs represent a simple and broadly applicable platform for robust tumor combination immunotherapy.

Cancer immunotherapy, such as ICB, has significantly improved the treatment outcomes for patients with many types of cancers.[1,2] Yet, most cancer patients still do not durably respond to current immune checkpoint inhibitors (ICIs) or suffer from immune-related adverse effects (irAEs) due to imbalanced immune homeostasis.[3–5] Cancer therapeutic vaccines hold great potential to elicit or expand antitumor immunity, making cancer vaccines appealing to improve the treatment outcome of ICB tumor immunotherapy. However, current cancer therapeutic vaccines have shown limited clinical efficacy,[6,7] largely due to the overall poor immunogenicity of tumor-associated antigens (TAAs) and neoantigens.[8] This demands innovative technologies to promote the ability of cancer vaccines to elicit antitumor immunity, especially antigen-specific $CD8^+$ cytotoxic T lymphocytes (CTLs) that are central to tumor immunotherapy.

The ability of vaccines to elicit or expand $CD8^+$ CTLs is hinged on the efficiency of antigen processing and cross-presentation by APCs.[9,10] Specifically, in the cytosol of APCs [e.g., dendritic cells (DCs)], vaccine antigens undergo ubiquitination, allowing for antigen processing into antigenic minimal epitopes by 26S proteasome via proteolytic cleavage.[11] The resulting minimal epitopes are then transported by transporter associated with antigen processing (TAP) from the cytosol into the endoplasmic reticulum, where minimal epitopes are complexed with major histocompatibility complex class I (MHC-I). Lastly, the MHC-epitope complexes are transported to APC cell surfaces, where epitopes are presented to $CD8^+$ T cells to elicit CTL responses.[12] The modulation of proteolytic cleavage kinetics of protein of interest has garnered tremendous attention over the past decade.[13–15] Notably, proteolysis targeting chimeras (PROTACs) have been studied to facilitate the degradation of endogenous target proteins for various biomedical applications, such as cancer therapy.[1,2] A PROTAC is comprised of a ligand for E3 ligase[17] and a ligand for protein of interest (POI), which promotes the physical proximity of E3 ligase with POI, thereby facilitating the ubiquitination and proteolytic cleavage of the latter.[18] Interestingly, recent evidence has emerged that PROTACs may promote antigen-specific immune responses against protein antigens[19] and antigenic peptides derived from target proteins for PROTAC[20]. Therefore, we hypothesize that facilitating the proteolytic processing of exogenous vaccine antigens into minimal peptide epitopes in APCs may promote the corresponding antigen presentation and antigen-specific $CD8^+$ CTL responses, thereby promoting their tumor therapeutic efficacy.

Here, we present PROTAVs as a vaccine platform that promotes antigen processing and cross-presentation in APCs, thereby promoting antitumor T cell responses for tumor combination immunotherapy (**Fig. 1**). A PROTAV is a modular molecular conjugate of a peptide or protein antigen, an E3 ligase-binding ligand, and a linker between the antigen and the E3 ligand. The E3 ligand avidly binds to endogenous E3 ligase, thereby bringing E3 ligase into proximity of antigens to facilitate antigen ubiquitination and proteolytic processing by proteasome. In APCs, PROTAVs facilitated antigen proteolytic processing, and promoted antigen presentation, thus potentiating antigen-specific T cell response. In mice, PROTAV elicited up to 3-fold antigen-specific $CD8^+$ T cell response relative to unmodified vaccine. PROTAVs are broadly applicable to common types of tumor antigens based on proteins, synthetic long peptides, and multivalent fusion peptides. In mice, a novel bi-adjuvant

of oligonucleotide agonists for cGAS and TLR9[21,22] empowered peptide-based PROTAV for potent systemic and tumor immunomodulation. In tumor-bearing mice, when co-delivered with cGAS/TLR9 agonists in LNPs, PROTAV, alone or combined with ICIs, not only promoted systemic antitumor immune responses, but also reduced tumor immunosuppression and promoted the tumor infiltration of antitumor T cells. In multiple murine tumor models, relative to benchmark protein or peptide vaccines, PROTAV significantly promoted ICB therapeutic efficacy of tumors, resulting in multiple-fold increase of the rates of tumor complete regression (CR). Remarkably, the combination of PROTAV and ICB eradicate most of large tumors that are otherwise resistant to even dual ICB therapy. These results demonstrate the potential of PROTAVs for robust tumor combination immunotherapy.

Results

Synthesis, linker optimization, and characterization of PROTAVs.

A PROTAV is a modular molecular conjugate of a protein/peptide antigen, an E3 ligase-binding ligand[23], and a linker in between (**Fig. 1, 2a**). Depending on their amino acid sequences, tumor protein/peptide antigens have heterogeneous physicochemical properties and chemical reactivities. Thus, a broadly applicable, biocompatible, simple, and efficient method for PROTAC synthesis is highly desirable for developing PROTAVs for cancer immunotherapy. To this end, we tested PROTAV synthesis via two biocompatible and efficient conjugation chemistries: 1) N-hydroxysuccinimidyl (NHS) and 1-ethyl-3-(3-dimethylaminopropyl) carbodiimide (EDC) conjugation of NHS-modified E3 ligand with the primary amines of amino acids in antigens, and 2) thiol-maleimide conjugation of maleimide-modified E3 ligand with thiol on cysteine in antigens. We expect that the ubiquitous amino acids with primary amines (e.g., lysine) and thiol (i.e., cysteine) would enable broad application of these methods for PROTAV synthesis. Moreover, the modular structure of PROTAVs allows for the site-specific addition of reactive amino acids into antigens for optimal conjugation with E3 ligands. Various molecular ligands for many E3 ligase subtypes, such as cereblon (CRBN), have been studied in PROTACs, including multiple clinical studies of CRBN-based PROTACs.[24–28] We chose pomalidomide, a commonly used CRBN ligand, as a representative E3 ligand in our PROTAV studies. Pomalidomide is an FDA-approved drug, which is expected to facilitate the clinical translation of pomalidomide-based PROTAV due to its clinically validated CRBN binding ability and the safety profile of pomalidomide.[26] Note that, the structural modularity of PROTAVs allows for easy adjustment of E3 ligands.[23,29] To synthesize PROTAVs, we first used chicken ovalbumin (OVA) as a model antigen, which can be proteolytically processed to generate a murine MHC-I-restricted minimal peptide epitope (SIINFEKL, $OVA_{257-264}$) to elicit $CD8^+$ T cell response.[30]

Linker chemistry can be critical for molecular conjugate therapeutics[31], including PROTACs[32]. We hypothesize that the linkers between E3 ligand and antigen in PROTAVs can be critical for its CRBN binding, antigen processing, and induction of T cell response. To screen for the optimal linker for PROTAV to elicit T cell response, we synthesized a series of PROTAVs with linkers of various water solubility (ethylene glycol or lipid)

and length (**Fig. 2b**). PROTAV-OVA was first synthesized via NHS-EDC conjugation in two steps (**Fig. 2a**). First, we conjugated pomalidomide to an NHS-modified linker, as verified by electrospray ionization mass spectrometry (ESI-MS) (**Supplementary Fig. 1**). The resulting pomalidomide-linker showed great biostability, with limited degradation of pomalidomide-EG_4 as an example after 2-hour incubation in serum, as measured by LC-MS (**Supplementary Fig. 2**). Second, we conjugated the resulting pomalidomide-linker-NHS with OVA via NHS conjugation with surface amines of OVA. The products were subject to ultracentrifugation purification. PROTAV-OVA synthesis was verified by 1) liquid chromatography-MS (LC-MS) (**Fig. 2c**), and 2) the presence of the characteristic UV-vis absorbance of pomalidomide (peak absorbance at 420 nm) in PROTAV-OVA (**Fig. 2d**). Conveniently, the linear correlation of pomalidomide absorption with PROTAV-OVA concentrations allows for easy estimation of the average pomalidomide copy numbers per PROTAV-OVA via UV-vis absorbance (**Supplementary Fig. 3a**). Next, by subcutaneous (*s.c.*) injection at tail base (day 0 and day 14), C57BL/6 mice were immunized with these PROTAV candidates individually, with unmodified OVA and PBS as controls and immunostimulant CpG-1826 oligonucleotide (a TLR9 agonist) (**Supplementary Table 1**) as adjuvant (**Fig. 2e**). H-$2K^b$/SIINFEKL tetramer staining (day 21, day 35) showed that, while all PROTAV-OVA(s) promoted the fraction of SIINFEKL-specific $CD8^+$ T cells among peripheral blood mononuclear cell (PBMC) $CD8^+$ T cells, PROTAV-OVA with a tetrameric ethylene glycol (EG_4) linker consistently elicited the highest T cell responses (**Fig. 2f**). Further, as shown by *ex vivo* antigen restimulation of PBMC T cells followed by intracellular cytokine staining (day 35), PROTAV-OVA with an EG_4 linker elicited the most multifunctional $CD8^+$ T cells that produced interferon-γ (IFN-γ) and tumor necrosis factor-α (TNF-α) (**Fig. 2g**). These results demonstrated that PROTAV-OVA with an EG_4 linker elicited a large quantity and a good quality of T cell responses. This, together with its relatively short length, allows EG_4 linker to be selected for further studies. Moreover, physical mixture of OVA and pomalidomide elicited comparable levels of SIINFEKL-specific $CD8^+$ T cell response relative to OVA alone (**Supplementary Fig. 4**). This not only verifies the benefit of covalent pomalidomide-antigen conjugation for T cell response, but also rules out the impact from the intrinsic immunomodulatory effect of pomalidomide on the ability of PROTAV to elicit T cell responses. In a molecular binding assay using nano isothermal titration calorimeter (ITC), PROTAV-OVA showed strong binding affinity with CRBN (dissociation constant K_d = 1.2 μM), in contrast to negligible binding between OVA and CRBN (**Fig. 2h, Supplementary Fig. 5**). Relative to pomalidomide binding to CRBN (K_d = 156 nM)[33], the reduced binding affinity between CRBN and pomalidomide in PROTAV-OVA is presumably caused by the structural hindrance of OVA for CRBN binding. Nonetheless, these results provide the basis for avid CRBN binding in APCs to facilitate antigen ubiquitination and proteolytic processing.

The copy number of E3 ligands per antigen can also be critical for their E3 ligase binding and antigen processing. To test PROTAV-OVA with varying pomalidomide copy numbers per antigen, we synthesized PROTAV-OVA with different pomalidomide-EG_4-NHS: OVA feeding molar ratios at 5: 1, 10: 1, 20: 1, and 30: 1, resulting in PROTAV-OVA with averages of 2.1, 6.3, 8.0, and 9.2 pomalidomide copies per OVA, respectively, as measured using a method of free-amine-reactive fluorescent labeling (**Supplementary Fig. 3b**). To study their T

cell responses, mice were immunized as above with CpG-adjuvanted PROTAV-OVA with different pomalidomide copies, respectively (**Fig. 2e**). H-2K^b/SIINFEKL tetramer staining revealed that a pomalidomide: OVA feeding ratio of 5:1 elicited one of the highest fractions of SIINFEKL-specific PBMC CD8$^+$ T cells (**Fig. 2i**). Consistently, PROTAV-OVA with pomalidomide: OVA feeding ratio of 5:1 also resulted in the most fraction of multifunctional cytokine-producing PBMC CD8+ T cells upon antigen restimulation (**Fig. 2j**). This, together with its simplicity of synthesis and quality control, allow us to choose this feeding ratio for further studies. Next, we compared NHS-EDC conjugation with thiol-maleimide conjugation for PROTAV synthesis, which conjugate pomalidomide with the intrinsic primary amine and thiol on antigens, respectively. UV-vis absorbance confirmed that comparable copy numbers of pomalidomides were grafted per OVA by the two methods (**Supplementary Fig. 3c**). After immunization of mice with the resulting PROTAV-OVA, H-2K^b/SIINFEKL tetramer staining confirmed that PROTAV-OVA synthesized using these two methods elicited comparable fractions of SIINFEKL-specific PBMC CD8$^+$ T cells (**Supplementary Fig. 6**).

PROTAVs facilitate antigen proteolysis and promote antigen cross-presentation in DCs *in vitro* and *in vivo*.

The proteolytic processing of protein/peptide antigens by 26S proteasome is a critical step in the antigen processing cascade prior to presentation of the resulting minimal antigen epitopes from APCs to T cells. We hypothesize that, by directly conjugating E3 ligands on antigens, PROTAVs enhance antigen ubiquitination, and thus expedite antigen processing and presentation, resulting in promoted T cell activation. We studied antigen proteolytic processing (*i.e.*, degradation) of PROTAVs using PROTAV-OVA prepared from a fluorogenic DQ-OVA conjugate. The DQ fluorescence of DQ-OVA is self-quenched until OVA degradation[34], allowing for a semi-quantitative study of OVA degradation. After treatment of DC2.4 cells with PROTAV-DQ-OVA *vs.* DQ-OVA for a series of durations up to 72 h, flow cytometry showed elevated DQ fluorescence of cells treated with PROTAV-DQ-OVA relative to DQ-OVA at the corresponding time points (**Fig. 3a-b**). We further studied this by confocal microscopy. After treatment of DCs as above for only 0.5 h, PROTAV-DQ-OVA started to show enhanced DQ fluorescence recovery relative to DQ-OVA (**Fig. 3c**). Following a 0.5-h treatment, cells were washed to remove extracellular PROTAV-OVA-DQ and then incubated for an additional 5 h. Confocal microscopy showed that, compared to the initial 0.5-h treatment, the ratio of cytosolic to endolysosomal DQ fluorescence in DCs increased after the extended incubation (**Fig. 3d**). This not only suggests enhanced antigen degradation by PROTAV at the subcellular levels, but also demonstrated effective delivery of PROTAV-OVA to the cytosol, which is required for antigens to bind to E3 ligase and undergo proteolytic processing. At the molecular level, western blot (WB) demonstrated that PROTAV-OVA facilitated OVA degradation relative to OVA in DCs (**Fig. 3e**). Mechanistically, co-immunoprecipitation (co-IP) showed that PROTAV enhanced the fraction of OVA and ubiquitin colocalization in

DCs, suggesting that PROTAV promoted OVA ubiquitination (**Fig. 3f**). These results suggest that PROTAV facilitated antigen proteolytic processing, a prerequisite for antigen presentation.

To study antigen presentation, C57BL/6 mouse-derived bone marrow-derived DCs (BMDCs) were treated with PROTAV-OVA *vs.* OVA for a series of durations of up to 24 h, followed by antibody staining and flow cytometric analysis of the complex of SIINFEKL and H-2K^b (an MHC-I subtype). CpG-1826 oligonucleotide, an agonist for murine TLR9,[22] was used as an immunostimulant adjuvant in the above vaccine. As a result, after treatment for 12 - 24 h, relative to OVA, PROTAV-OVA enhanced the level of H-2K^b/SIINFEKL on DCs, suggesting that PROTAV promoted antigen presentation (**Fig. 3g**). Note that, relative to OVA, PROTAV-OVA did not significantly enhance SIINFEKL presentation until 12 h after treatment. This is likely because the cytosolic delivery of OVA or PROTAV-OVA is time-consuming and inefficient, involving endocytosis and endosome escape; and shortly after treatment, pre-existing E3 ligases suffice to efficiently process both OVA and PROTAV-OVA that have reached the cytosol. Further, proteasome inhibitor (MG132)[35] reduced the level of SIINFEKL presentation on DCs treated with PROTAV-OVA or OVA as above (**Fig. 3h**), verifying that PROTAV enhances antigen presentation in a proteasome-dependent manner. To study this *in vivo*, C57BL/6 mice were *s.c.* injected at tail base with PROTAV-OVA *vs.* OVA, with CpG adjuvant. After up to 4 days, analysis of draining inguinal lymph nodes revealed that PROTAV-OVA elevated SIINFEKL presentation levels on intranodal DCs throughout this course (**Fig. 3i**). To further study PROTAV-treated DCs for antigen presentation to T cells, BMDCs were treated as above with CpG-adjuvanted PROTAV-OVA *vs.* OVA for 24 h, and then cocultured with CSFE-stained OT-1 CD8$^+$ T cells for 96 h. As shown by flow cytometry, OT-1 CD8$^+$ T cells cocultured with PROTAV-OVA-treated DCs underwent significantly more CSFE signal dilution and cell division (**Fig. 3j-k**). This suggests that PROTAV-OVA enhanced antigen presentation from DCs to promote T cell activation. For further mechanistic understanding, we employed RNA sequencing (RNA-seq) for transcriptomic analysis of BMDCs treated with CpG-adjuvanted PROTAV-OVA or OVA, respectively. Gene ontology (GO) enrichment analysis revealed that, relative to OVA, PROTAV-OVA significantly activated the ubiquitin and immune response-related pathways (**Supplementary Fig. 7**). Taken together, these data demonstrated that PROTAV promoted proteasome-dependent antigen proteolytic processing, facilitated antigen presentation, and enhanced T cell activation, providing the basis for PROTAV to promote T cell response.

PROTAV-E7 elicited potent HPV E7-specific T cell responses for robust combination immunotherapy of large HPV-associated tumors in mice.

Depending on the amino acid sequences, protein or peptide antigens have highly heterogeneous tertiary structures and structurally accessible amino acids for E3 ligand conjugation. Synthetic long peptides, which contain the minimal peptide epitopes to elicit antitumor T cell responses, are extensively studied in cancer therapeutic vaccines. Relative to minimal peptide epitopes, synthetic long peptide antigens allow for de novo

antigen processing and complexation with MHC in APCs for potent T cell activation with minimal tolerance.[36,37] To explore the applicability of PROTAVs in synthetic long peptide antigens, we first studied PROTAV for HPV16 oncoviral antigen E7. High-risk HPV, such as HPV16 and HPV18, causes ~5% of all cancer cases worldwide, including 90% of cervical and anal cancers.[38] Current HPV prophylactic vaccines are unable to treat HPV-associated cancer,[38–40] and ICB has limited therapeutic efficacy in HPV-associated cancers. Therapeutic vaccines are promising to elicit $CD8^+$ T cell response, thereby controlling HPV-associated cancer. HPV16 protein E7 is an ideal Ag because 1) E7 is consistently expressed in HPV-associated cancer, but not healthy cells, providing selectivity; 2) E7 is required to initiate and maintain HPV-associated cancer, preventing cancer immune escape; and 3) as an oncoviral antigen, E7 bypasses host immune tolerance.[41–48] Although E6-targeted adoptive T cell receptor (TCR)-engineered T cell therapy has shown promising therapeutic efficacy for HPV-associated cancer,[49] conventional E7-based therapeutic vaccines showed limited tumor therapeutic efficacy in the clinic thus far, in part due to the suboptimal immunogenicity of E7. Approaches that potentiate E7 immunogenicity are therefore highly desired for developing E7-based therapeutic vaccines.

To this end, we studied PROTAV-E7 to potentiate E7 immunogenicity for HPV-associated cancer immunotherapy. To synthesize PROTAV-E7, we used synthetic long peptide antigen $E7_{39\text{-}98}$ (denoted as E7 thereafter) (**Fig. 4a**), in which $E7_{49\text{-}57}$ (RAHYNIVTF) is a murine H-$2D^b$-binding minimal epitope. As predicted by AlphaFold3,[50] most of the preexisting cysteines in E7 have good spatial accessibility, which is expected to allow for their chemical conjugation with maleimide-EG_4-pomlidomide (**Fig. 4b**). Thus, as verified by LC-MS (**Supplementary Fig. 8**), we synthesized PROTAV-E7 by conjugating the preexisting cysteines in E7 with maleimide-EG_4-pomalidomide under a reductive condition to prevent dithiol formation from two adjacent cysteines. To identify the pomalidomide conjugation sites on E7, PROTAV-E7 was treated with proteinase, followed by LC-tandem MS proteomics analysis. We found that C61 was the primary conjugation site of maleimide-EG_4-pomalidomide (**Fig. 4c, Supplementary Table 2**). The finding that $E7_{49\text{-}57}$ was not conjugated with pomalidomide rules out the potential risk of the loss of MHC binding ability by pomalidomide-conjugated $E7_{49\text{-}57}$. Peptides, including $E7_{39\text{-}98}$ and PROTAV-$E7_{39\text{-}98}$, often have low water solubility and poor delivery efficiency to lymphoid tissues, such as draining lymph nodes where APCs process and present antigens to T cells. Moreover, peptide vaccines are overall poorly immunogenic, which demands immunostimulant adjuvants to elicit T cell responses. Yet, many of current molecular adjuvants, including TLR agonists such as CpG, still elicit suboptimal T cell responses when used together with peptide antigens. This is in part because of their limited ability to elicit type-I IFN response, which is critical to elicit T cell response. Lastly, a physical mixture of peptide antigens and adjuvants often randomly disseminates with poor co-delivery to lymphoid APCs, causing suboptimal T cell responses. To address these issues, first, we recently developed an oligonucleotide-based cGAS agonist, Svg3.[21] Svg3 selectively activates murine and human cGAS to elicit strong type-I IFN responses. Thus, we combine Svg3 and CpG as bi-adjuvant for PROTAV to concurrently activate cGAS and TLR9, thereby eliciting potent T cell responses. Second, we used ionizable SM-102 LNPs, which have been used in COVID-19 mRNA vaccine

Spikevax, as nanocarriers to co-load PROTAV-E7 and adjuvants Svg3 and CpG. Vaccine-loaded LNPs were synthesized via rapid microfluidic mixing, with the Svg3: CpG molar ratio of 1:2 and an overall N:P ratio of 6:1. The resulting PROTAV-E7/Svg3/CpG-loaded LNPs displayed hydrodynamic diameters of 148 ± 5 nm (mean ± SD) with great homogeneity (PDI: 0.145), as measured by hydrodynamic light scattering (DLS) (**Fig. 4d**). Cryogenic electron microscopy (cryo-EM) further revealed the exterior and internal morphology of PROTAV-E7/Svg3/CpG-loaded LNPs (**Fig. 4d**).

We then studied the resulting PROTAV vaccines (i.e., PROTAV-E7/Svg3/CpG-loaded LNPs) to elicit E7-specific T cell responses. C57BL/6 mice were *s.c.* injected at tail base with PROTAV-E7, with E7 and PBS as controls (day 0, day 14). H-2D^b/E7$_{49-57}$ tetramer staining (day 21) showed that PROTAV-E7 elicited 13% E7-specific T cells among total live PBMC CD8$^+$ T cells, which is 2-fold of that elicited by E7 (7%) (**Fig. 4e**). When co-delivered with PROTAV-OVA, bi-adjuvant (Svg3 + CpG) elicited a higher number of E7-specific T cells than each mono-adjuvant (**Supplementary Fig. 9**), demonstrating the benefit of bi-adjuvant for these vaccines. Moreover, upon restimulation of PBMC T cells, intracellular cytokine staining revealed that PROTAV-E7 promoted the production of IFN-γ and TNF-α by CD8$^+$ T cells (**Fig. 4f**). These data demonstrated that PROTAV-E7 promoted the quantity and quality of E7-specific CD8$^+$ T cells, suggesting the ability to potentiate the immunogenicity of E7 in mice. Immune memory is critical for long-term tumor therapeutic efficacy and prevent tumor recurrence. PROTAV-E7 promoted the fraction of central memory T cells (CD44$^+$CD62L$^+$) (Tcm) and effector memory T cells (CD44$^+$CD62L$^-$) (Tem) among total PBMC CD8$^+$ T cells (**Fig. 4g, Supplementary Fig. 10**). The E7-specific T cell memory was verified by the observation that all mice immunized with PROTAV-E7 resisted the challenge of E7-positive TC-1 tumor cells *s.c.* administered 60 days after immunization (**Supplementary Fig. 11a**). Moreover, PROTAV-E7 upregulated the expression of immune checkpoints, such as programmed death receptor 1 (PD-1), on total CD8$^+$ T cells as well as E7-specific CD8$^+$ T cells (**Fig. 4h**), presumably due to innate and adaptive the immunostimulation as well as enhanced antigen exposure for T cells, especially for PROTAV. This suggests that PROTAV sensitized immune checkpoints for ICB therapy, providing the basis to combine ICB with PROTAV for optimal tumor therapeutic efficacy.

Motivated by the ability of PROTAV to potentiate E7 immunogenicity, we then evaluated PROTAV-E7, alone or combined with ICB (αPD-1), for the immunotherapy of TC-1 tumor in C57BL/6 mice. Mice with *s.c.* TC-1 tumor (50 mm^3) were treated with CpG-adjuvanted PROTAVs *vs.* controls (**Fig. 4i**). Relative to E7, PROTAV-E7 alone, already significantly retarded TC-1 tumor growth; remarkably, the combination of αPD-1 with PROTAV-E7 further facilitated the tumor regression and promoted the therapeutic response. As a result, within 60 days, PROTAV-E7 + αPD-1 eradicated 7/8 tumors, in contrast to 4/8 by PROTAV-E7 or E7 alone (**Fig. 4j, k**). PROTAV-E7 + αPD-1 had not yet reached the median mouse survival within 130 days after tumor inoculation. 30 days after tumor eradication, CD44 and CD62L staining revealed that relative to E7, PROTAV-E7 immunization promoted the fraction of CD44$^+$CD62L$^+$ Tcm cells among PBMC CD8$^+$ T cells (**Fig. 4l, m**). To verify antitumor immune memory, which is pivotal to prevent tumor recurrence, on day 60, mice with tumor CR were re-challenged with

TC-1 tumor cells. All these mice resisted this tumor challenge, demonstrating long-term antitumor immune memory elicited by these therapies (**Supplementary Fig. 11b**).

We then assessed PROTAV-E7, alone or combined with ICIs, for the immunotherapy of large tumors. Relative to small tumors, large tumors are substantially more challenging for immunotherapy to eradicate, largely due to hostile TME and systemic immunosuppression, and the demand for immunotherapy to elicit a large quantity and good quality of antitumor immunity for tumor eradication. Unfortunately, HPV-associated tumors are often already large at the time of diagnosis. We then used large TC-1 tumors (300 mm^3 at treatment initiation, 1.2-1.5% body weight) in syngeneic C57BL/6 mice to study PROTAV-E7 for ICB combination immunotherapy (**Fig. 4n**). For optimal therapeutic outcome, dual ICIs of αPD-1 and antibody against cytotoxic T lymphocyte antigen-4 (αCTLA-4) were used for combination immunotherapy with PROTAV-E7 vaccines. These large tumors did not significantly respond to the combination of E7 vaccines with αPD-1 + αCTLA-4, or αPD-1 + αCTLA-4 alone (**Fig. 4o, p**). Consistently, relative to control PBS treatment, αPD-1 + αCTLA-4 or E7 + αPD-1 + αCTLA-4 did not prolong the median mouse survivals (19 days). By contrast, combining PROTAV-E7 with αPD-1 + αCTLA-4 resulted in 4/8 eradication of these large ICI-resistant tumors, and mice had not reached the median survival yet within 40 days after tumor inoculation (**Fig. 4o, p**). During the treatment course, mouse body weights were not significantly changed by any of these treatments, indicating their promising safety profile (**Supplementary Fig. 12a**). Hematoxylin and Eosin (H&E) staining of the major organs from the above mice verified the promising safety of these treatments (**Supplementary Fig. 12b**). Taken together, these results demonstrated the potential of PROTAV-E7 for ICB combination immunotherapy of HPV-associated cancers.

Multivalent PROTAV elicited potent antigen-specific T cell responses

Melanoma represents the most prevalent skin cancer, and advanced melanoma has a <30% 5-year survival rate. Though ICB[3,5,51] has improved melanoma treatment outcomes, most melanoma patients do not respond to ICB[52,53] or suffer from irAEs.[3–5] Cancer therapeutic vaccines can improve ICB therapeutic efficacy by inducing antitumor immune cells as ICB targets, upregulating immune checkpoints, and reducing tumor immunosuppression.[54–58] To study PROTAV for melanoma, we designed a trivalent antigenic fusion peptide, TgT, for three long peptides of MHC-I melanoma TAAs: **T**rp2$_{175-194}$, **g**p100$_{16-35}$, and **T**rp1$_{450-469}$ (sequence and structure in **Fig. 5a-b**).[59–62] Multiple terminal K and C were added to promote pomalidomide conjugation via maleimide-thiol conjugation and ubiquitination on lysine, respectively. While such synthetic long fusion peptides have shown the benefit to elicit T cell responses with minimal immune exhaustion,[63] they must be proteolytically processed before effective antigen presentation. We expect TgT to elicit multi-specific $CD8^+$ T cells to overcome tumor antigen heterogeneity and the associated immune escape for optimal melanoma therapeutic efficacy.[36,64] PROTAV-TgT was synthesized by thiol-maleimide conjugation using pomalidomide-EG_4-maleimide (**Supplementary Fig. 13**). We again synthesized LNPs co-loaded with PROTAV-TgT and CpG/Svg3 adjuvants (CpG: Svg3 molar ratio: 2:1.

N:P ratio: 6:1.). DLS and cryo-EM showed that the sizes of the resulting LNPs are 157 ± 5 nm (mean ± SD) in diameter (PDI: 0.128), which is expected to allow for efficient delivery into draining lymph nodes (**Fig. 5c**).

Next, we studied the PROTAV-TgT to elicit T cell responses. C57BL/6 mice were immunized with PROTAV-TgT and TgT vaccines, respectively (*s.c.* at tail base, day 0 and day 14), with CpG and Svg3 adjuvants coloaded in LNPs (**Fig. 5d**). On day 21, PBMC T cells were analysed by flow cytometry to assess TgT-specific T cell responses. Specifically, gp100/H-2D^b tetramer staining showed that relative to TgT, PROTAV-TgT promoted gp100-specific CD8$^+$ T cell responses (**Fig. 5e, f**). Moreover, intracellular cytokine staining revealed that PROTAV-TgT promoted multifunctional CD8$^+$ cell responses (**Fig. 5g, h**). Immunoactivation and antigen exposure may upregulate the expression level of immune checkpoints, thereby sensitizing the corresponding ICB therapy. Indeed, immunization of mice with PROTAV-TgT vaccines upregulated the expression levels of PD-1 and T-cell immunoglobulin and mucin domain 3 (Tim-3) on total live PBMC CD8$^+$ T cells (**Fig. 5i, j)**. This provides the rationale for combining PROTAV with ICB (e.g., αPD-1) for optimal melanoma therapeutic efficacy. Moreover, flow cytometry analysis of CD44 and CD62L levels on PBMC CD8$^+$ T cells demonstrates that PROTAV-TgT elicited great CD8$^+$ T cell memory relative to TgT (**Supplementary Fig. 14**).

PROTAV-TgT, in combination with ICIs, elicited systemic antitumor immunity and remodeled the tumor immune microenvironment for robust melanoma immunotherapy.

Tumor microenvironment (TME) is primarily where tumor cells suppress antitumor immunity.[65] In addition to systemic antitumor immunomodulation, modulating the tumor immune milieu is pivotal to reducing immunosuppression and promoting tumor immunotherapeutic efficacy.[66] Using a B16F10 melanoma mouse model, we studied the systemic and TME immunomodulation by PROTAV-TgT, alone or combined with ICIs. Tumors were *s.c.* inoculated on mouse flank. Immunotherapy was initiated when tumor sizes reached *ca.* 50 mm^3. Specifically, mice were immunized *s.c.* at tail base with PROTAV-TgT, with PBS or TgT as controls. One day later, mice were treated with αPD-1 by *i.p.* administration. ICB was initiated one day post immunization to minimize antitumor T cell immune exhaustion caused by ICB prior to the antitumor T cell responses elicited by immunization. After two doses of vaccines and three doses of αPD-1, tumors, lymph nodes, along with PBMCs were collected for immune analysis (**Fig. 6a**). We first analyzed gp100-specific CD8$^+$ T cells in tumors using gp100/H-2D^b tetramer staining. Relative to TgT, PROTAV-TgT, alone or combined with ICIs, respectively, promoted the tumor infiltration of gp100-specific CD8$^+$ T cells (**Fig. 6b**). Importantly, relative to TgT + αPD-1, PROTAV-TgT + αPD-1 promoted the fraction of granzyme B-producing CD8$^+$ T cells among total CD8$^+$ T cells in melanoma (**Fig. 6c, Supplementary Fig. 15a**). Moreover, the ratio of CD8$^+$ T cells over regulatory T cells (Treg) (CD8$^+$/Treg) in tumor, which is predictive for effective tumor immunotherapy, was enhanced by PROTAV-TgT + αPD-1 (**Supplementary Fig. 15b**). Importantly, relative to PROTAV-TgT or αPD-1 alone, PROTAV-TgT + αPD-1 reduced the fractions of PD-1$^+$ intratumoral CD8$^+$ T cells and the PD-1 expression level on these cells, and reduced the number of intratumoral terminally exhausted PD-1$^+$Tim-3$^+$ CD8$^+$ T cells that are featured with reduced

proliferative capacity, diminished antitumor cytokine production, and impaired antitumor cytotoxic activity (**Supplementary Fig. 15c-d**). Collectively, these results suggested that PROTAV-TgT + αPD-1 promoted the antitumor cell density and functionality in TME. We then studied the systemic immunomodulation in peripheral blood and lymph nodes in the above treated mice. Again, gp100/H-2D^b tetramer staining of PBMCs showed that, relative to TgT, PROTAV-TgT, alone or combined with αPD-1, elevated the fraction of gp100-specific CD8$^+$ T cells among PBMC CD8$^+$ T cells (**Fig. 6d**). Similarly, relative to TgT, PROTAV-TgT, alone or combined with αPD-1, promoted the lymph node infiltration gp100-specific CD8$^+$ T cells (**Fig. 6e**). Further, PROTAV-TgT promoted the activation of conventional DC class 1 (cDC1) in lymph nodes, demonstrating the role of cDC1 in the activation of TgT-specific CD8$^+$ T cell responses by PROTAV-TgT (**Fig. 6f**). Overall, these results demonstrate that PROTAV-TgT, especially when combined with ICIs, increased antitumor immunity and reduced immunosuppression in TME while activating systemic antitumor T cell responses in tumor-bearing mice.

Encouraged by the ability of PROTAV-TgT for TME and systemic antitumor immunomodulation in tumor-bearing mice, we then assessed PROTAV-TgT, alone or combined with ICB (i.e., αPD-1), for melanoma therapy in a *s.c.* B16F10 melanoma mouse model. 3 days post tumor inoculation (tumor sizes: ca. 50 mm^3), mice started to be treated with: 1) PROTAV-TgT, with PBS or TgT as controls (*s.c.* immunization at tail base, days 3, 9, 15, 21), and 2) αPD-1 (*i.p.* administration, day 5, 8, 11, 14, 17, 20, 23) (**Fig. 6g**). PROTAV-TgT or TgT were co-loaded with CpG and Svg3 in SM-102 LNPs. Tumor volumes and mouse survivals were then monitored. Tumor growth curves showed that, relative to TgT, PROTAV-TgT alone already showed slightly stronger inhibition of tumor growth (**Fig. 6h-j**). Interestingly, when combined with ICIs, PROTAV-TgT significantly facilitated the tumor regression and promoted the therapeutic response in B16F10 melanoma in syngeneic mice. Specifically, Consistently, Kaplan-Meier mouse survival curves showed that PROTAV-TgT + αPD-1 resulted in significant survival benefits over controls such as PROTAV-TgT or ICIs alone, or TgT + αPD-1 combination. PROTAV-TgT + αPD-1 resulted in 4/8 tumor CR and long-term mouse survival without recurrence, in contrast to 1/8 for PROTAV-TgT and none for the other treatments (**Fig. 6i**). The median survival of mice treated with PROTAV-TgT + αPD-1 reached 58 days, a two-fold increase over TgT + αPD-1, PROTAV-TgT, or αPD-1. Meanwhile, PROTAV-TgT + αPD-1 did not cause any significant mouse body weight changes relative to control treatments (**Supplementary Fig. 16**), suggesting the promising safety of this treatment strategy. Collectively, these results clearly demonstrated that PROTAV-TgT promoted the ICB combination therapeutic efficacy of melanoma.

Discussion

Cancer therapeutic vaccines can elicit antitumor CD8$^+$ T cells that are pivotal for various approaches to tumor therapy, such as ICB. The antigens in cancer therapeutic vaccines often need to be proteolytically processed for MHC binding, antigen presentation, thereby priming naïve T cells or expanding pre-existing antigen-specific T cells. We developed PROTAVs as a novel platform to facilitate proteolysis and thus promote antitumor T cell

responses for cancer immunotherapy. To the best of our knowledge, this is the first time that the ability of vaccines to elicit antitumor T cell responses can be promoted by ligand-medicated E3 ligase engagement that promotes antigen ubiquitination, proteolytic processing, and presentation. While PROTAC represents an emerging platform for the degradation of endogenous intracellular proteins, our PROTAV is the first technology that promotes the proteolysis of exogenous proteins/peptides. We envision that the research and development of PROTAC over the past two decades would facilitate the research and development of PROTAV. PROTAVs hold the potential for rapid development and clinical translation. This is supported by the potential of cancer therapeutic vaccines, the vast unmet clinical need for novel and effective cancer immunotherapeutic approaches, and the clinically proven efficacy and safety of PROTACs for molecular ligand-promoted proteolysis in multiple clinical trials.

With a modular structure that can be easily synthesized via biofriendly conjugation, PROTAVs allow for easy adjustment of E3 ligands, linkers, and various protein/peptide antigens. In this study, we used pomalidomide, a CRBN ligand as a representative E3 ligand. Pomalidomide is an FDA-approved immunomodulatory drug interacting with CRBN and inducing degradation of essential Ikaros transcription factors.[26] Physically mixing pomalidomide with OVA did not significantly impact the anti-OVA T cell responses, ruling out the confounding immunomodulatory effect of pomalidomide in PROTAV. We expect that the clearly understood pharmacology, toxicology, and safety profile of pomalidomide, as well as ongoing clinical studies of pomalidomide-based PROTACs, would facilitate the clinical translation of PROTAV. Moreover, alternative E3 ligands (e.g., VH032 for Von Hippel-Lindau (VHL), cIAP1 for inhibitor of apoptosis proteins (IAP))[29] can be readily tested in PROTAV. Site-specific conjugation of E3 ligands on antigens can be desirable to not only avoid conjugating these ligands on antigenic minimal epitopes and affecting the MHC binding ability of these epitopes, but also for reproducible batch-to-batch manufacturing. Here, we explored pomalidomide conjugation on natural amino acids, primarily lysine and cysteine. While lysine conjugation may lead to competition for the use of lysine between E3 ligand conjugation and ubiquitination, maleimide-cysteine conjugation may bypass such complication. Moreover, we envision that unnatural amino acids can be site-specifically incorporated into protein/peptide antigens, allowing for bioorthogonal site-specific conjugation of E3 ligand on unnatural amino acids in antigens without affecting any minimal antigenic epitopes[67,68].

PROTAVs could have broad applications in proteins or synthetic long peptide vaccines. Relatively to whole proteins, synthetic long peptides contain minimal peptide epitopes to elicit antitumor T cell responses and can have the advantage of large-scale manufacturing and high pharmaceutical stability. Relative to minimal peptide epitopes, synthetic long peptide antigens allow de novo antigen processing in APCs for potent and durable immunomodulation with minimal tolerance, the latter of which can be caused by MHC presentation of antigen epitopes from APCs to T cells in the absence of co-stimulation or proinflammatory cytokines.[36,37] Further, the simple and efficient biocompatible conjugation of E3 ligands on tumor antigens permits their easy adoption into current protein/peptide vaccines, such as tumor-associated antigens, tumor neoantigens, and oncoviral

antigens. Multivalent antigen vaccines are poised to be used for tumor immunotherapy because 1) they could overcome the complications associated with the vast intra-patient and inter-patient tumor antigenic heterogeneity and the resulting tumor immune escape, and 2) the use of both MHC-I and MHC-II classes of antigens yields the optimal tumor therapeutic efficacy. To leverage the benefits of multivalent antigen vaccines, multivalent antigens need proteolytic processing to generate minimal antigen epitopes to bind MHC and activate T cell responses. For instance, multivalent vaccines hold the potential to treat cancer associated with various serotypes of HPV. High-risk HPV, such as HPV 16 and 18, causes ~5% of all cancer cases worldwide, including 90% of cervical and anal cancers.[38] Although prophylactic HPV vaccines prevent persistent HPV infection and pre-cancerous lesions, the prevalence of HPV-related cancers is still staggering due to the limited public uptake of these vaccines. Moreover, these prophylactic vaccines are unable to treat HPV-associated cancer.[38–40] ICB and adoptive cell transfer therapies for HPV-associated cancer are limited by ICB resistance and unsustainable memory T cell immunity. Therapeutic vaccines are promising to elicit $CD8^+$ T cell response for HPV-associated cancer immunotherapy. Conventional HPV E7-based experimental therapeutic vaccines have limited efficacy against HPV lesions in the clinic so far, in part due to suboptimal immunogenicity. HPV16 E7 not only includes an H-$2D^b$-binding epitope for preclinical research in mice, but also has a clinically-validated antigen epitope ($E7_{11-19}$)[49] for human leukocyte antigen (HLA)-A02:01, one of the most prevalent HLA haplotypes. This is expected to facilitate the clinical translation of E7-based vaccines from preclinical evaluation.

Protein/peptide vaccines demand immunostimulant adjuvants to elicit optimal innate and adaptive immunity. In this study, we studied Svg3 and CpG bi-adjuvant in peptide PROTAV for tumor combination immunotherapy. Previously, we engineered Svg3 oligonucleotide as a potent and selective cGAS agonist that can elicit type-I IFN responses, which are instrumental to eliciting T cell responses. The cationic charges of Svg3 and CpG oligonucleotides as well as the hydrophobic many peptides, especially when conjugated with pomalidomide, allows for easy co-loading into LNPs. Although ionizable LNPs are immunostimulatory to elicit potent antibody responses,[69] their ability to potentiate T cell responses can be further improved. Our study also suggests the potential of CpG and Svg3 as combination adjuvants to potentiate LNP-based vaccines to elicit T cell responses. Taken together, these results support the potential of PROTAVs as a novel platform of cancer therapeutic vaccines for broad application in the robust immunotherapy of many types of cancer.

Methods

PROTAV synthesis and characterization

Pomalidomide-linker-NHS. A series of linkers (e.g., EG_4) was used in pomalidomide-linker-COOH (Tocris Bioscience, Minneapolis, MN) as starting materials. Pomalidomide-linker-COOH (2.0 mg, 3.8 µmol), NHS (0.5 mg, 4.3 µmol), and EDC hydrochloride (3.9 mg, 20.3 µmol) were added into a glass vial with 100 µL anhydrous dimethylformamide (DMF) and stirred at room temperature for 2 hours. After that, DMF was evaporated and 500 µL chloroform was added into the vial. The mixture was washed with H_2O twice, the organic phase was collected, and the solvent was removed under vacuum to obtain pomalidomide-linker-NHS. Then Pomalidomide-linker-NHS (0.8 mg), antigen peptide or protein (11.0 mg) were added into a glass vial with 1 mL phosphate-buffered saline (pH 8.0) and stirred at room temperature for 2 hours. After that, the PROTAV was purified by ultrafiltration (10-kDa cutoff; Millipore). Fluorescence spectra (BioTek Cytation 5; with fluorescamine as a probe)[70] or LC-MS (Thermo Scientific) was used to analyze the copy numbers of pomalidomide-linker conjugated per antigen peptide or protein molecule.

Pomalidomide-EG_4-maleimide. Pomalidomide-EG_4-NH_2 (2 mg, 3.7 µmol) and maleic anhydride (0.7 mg, 7.1 µmol) were added into a glass flask with 1 mL chloroform and refluxed with stirring (60 °C, 24 h). Then, chloroform was evaporated, and acetic anhydride (1 mL) and sodium acetate (0.7 mg, 7.5 µmol) were added into the flask. The reaction solution was refluxed with stirring (90 °C, 24 h). Next, the reaction solution was washed with 1 M aqueous sodium hydroxide solution. The organic phase was extracted by dichloromethane. The solvent was removed under vacuum to obtain pomalidomide-EG_4-maleimide. Next, pomalidomide-EG_4-Mal (0.8 mg) and peptide/protein antigen (11.0 mg) were added into a glass vial with 1 mL H_2O (pH 7.0) and stirred at room temperature (4 h). Lastly, PROTAV was purified by ultrafiltration (10 kDa cutoff; Millipore) and verified by UV-vis and LC-MS.

Mapping of conjugation sites of pomalidomide on peptides by LC-Tandem MS

In-solution digestion. PROTAV-E7 prepared as above was submitted to Proteomics Resource Facility at University of Michigan for analysis using their optimized protocols. Briefly, the cysteines were reduced with 10 mM DTT (45° C for 30 min) and alkylated with 65 mM 2-Chloroacetamide, for 30 min at room temperature. Overnight digestion with 1 µg sequencing grade, modified trypsin or Glu-C was carried out at 37° C with constant mixing (ThermoMixer). Digestion was stopped by acidification and peptides were desalted using SepPak C18 cartridges using manufacturer's protocol (Waters). Samples were completely dried using vacufuge.

LC-Tandem MS. The resulting peptides were dissolved in 9 mL of 0.1% formic acid/2% acetonitrile solution. 2 µL of the resulting peptide solution was resolved on a nano-capillary reverse phase column (EasySpray PepMap C18, 2 µm, 50 cm, #ES903, Thermo Scientific) using a 0.1% formic acid/acetonitrile gradient at 300 nL/min over a period of 90 min. Eluent was directly introduced into *Q Exactive HF* mass spectrometer

(Thermo Scientific, San Jose CA) using an EasySpray source. MS1 scans were acquired at 60K resolution (AGC target = 3 x 10^6; max IT = 50 ms). Data-dependent collision induced dissociation MS/MS spectra were acquired on 20 most abundant ions following each MS1 scan (NCE ~28%; AGC target 1 x 10^5; max IT 45 ms).

Database search. Proteins were identified by searching the data against common Repository of Adventitious Proteins (cRAP) database and the antigens in PROTAVs using Proteome Discoverer (v3.0, Thermo Scientific). Search parameters included MS1 mass tolerance of 10 ppm and fragment tolerance of 0.1 Da; two missed cleavages were allowed; oxidation of methionine, deamidation of aspergine and glutamine, carbamidimethylation or conjugation of pomalidomide (572.21 Da) of cysteine were considered as potential modifications. False discovery rate (FDR) was determined using FixedPSM validator and proteins/peptides with a delta Cn of 0.05 were retained for further analysis. Spectra assigned to pomalidomide modification were manually verified, when possible.

Nano ITC measurement of PROTAV-CRBN binding

The binding affinity assay was performed using NanoITC (TA Instruments). Incremental titration (20, 2.5 µL injections in every 300 s) of CRBN protein (7.5 µM) into PROTAV-OVA (100 µM) was used for the assay. Background titration was performed using same titration method to subtract the heat from protein buffer. The ITC thermogram was analyzed using NanoAnalyze, and the Nano ITC data was fit into a one site-specific binding model in GraphPad to determine the K_d .

Plasma stability study of pomalidomide-EG_4-COOH

The *in vitro* stability of pomalidomide-EG_4-COOH was studied in CD1 mouse plasma (Innovative Research Inc, Novi, US). Pomalidomide-EG_4-COOH powder was weighed and dissolved in DMSO to a working concentration of 100 µM. 495 µL of pre-warmed plasma at 37 °C was prepared followed by spiking 5 µL of the 100 µM pomalidomide-EG_4-COOH working solution, to a final concentration of 1 µM. The spiked mouse plasma was incubated at 37 °C for 4 h. 40 µL plasma samples were separately acquired at 0, 5, 10, 15, 30, 45, 60, 120, and 240 min, and reactions were rapidly terminated by adding 160 µL of cold acetonitrile containing internal standard (10 ng/mL IPI549 in acetonitrile) at each time point. After quenching, the samples were shaken for 5 min at 700 rpm and centrifuged at 4000 rpm for 10 min. 100 µL of the supernatant from each well was transferred into a 96-well sample plate for LC/MS analysis. The *in vitro* plasma half-life ($t_{1/2}$) was calculated using the expression $t_{1/2}$ = 0.693/b, where b is the slope found in the linear fit of the natural logarithm of the fraction remaining of the test compound vs. incubation time.

Western blotting (WB)

WB was employed to investigate the intracellular degradation of PROTAV-OVA. DC2.4 cells were treated with PROTAV-OVA or OVA. Subsequently, the cells were harvested and lysed in RIPA lysis buffer (comprising 50 mM Tris-HCl, pH 7.4, 150 mM NaCl, 1% NP-40, and 0.1% SDS), with the addition of 1 mM phenylmethylsulfonyl

fluoride to inhibit protease activity. The lysates were then centrifuged at 12,000 g for 10 minutes at 4°C, and the supernatants were collected as the protein fraction. Protein concentrations were measured using a BCA protein assay kit, after which the samples were denatured at 70 °C for 15 minutes in the presence of 25% (v/v) loading buffer. Proteins were subsequently separated *via* SDS-polyacrylamide gel electrophoresis (SDS-PAGE) and transferred to a polyvinylidene fluoride (PVDF) membrane (Merck Millipore). To prevent non-specific binding, the membrane was blocked with 5% non-fat dry milk in Tris-Buffered Saline with Tween 20 (TBST) for 1 hour at room temperature, followed by overnight incubation at 4°C with the primary antibody, diluted 1:1000 in 5% non-fat dry milk. The samples were then incubated with an HRP-conjugated secondary antibody, diluted 1:5000 in 5% non-fat dry milk, for 1 hour at room temperature. OVA was analyzed using a BioRad GelDoc imaging system.

Co-IP

Co-IP was used to evaluate the interaction between OVA and ubiquitin. DC2.4 cells were treated with PROTAV-OVA and OVA, respectively, for 12 - 16 h. Proteins were extracted from as-treated cells using a magnetic IP/co-IP kit (Thermo Fisher Scientific, Waltham, MA). The protein lysates were incubated with anti-OVA magnetic beads for 2 - 3 h. The beads were then washed for four times using a buffer of 50 mM Tris-HCl (pH 7.5), 150 mM NaCl, 20% glycerol, 0.1% Triton X-100, and 1 mM EDTA (pH 8.0). The immunoprecipitates were resolved via SDS-PAGE, transferred to a PVDF membrane (Merck Millipore), and subsequently probed with anti-ubiquitin antibodies. Ubiquitin analysis on the resulting gel was detected using a BioRad GelDoc imaging system.

PROTAV LNP preparation

PROTAV LNPs were synthesized using microfluidic chips on a NanoGenerator Flex-S instrument (PreciGenome, San Jose, CA). An ethanol phase containing peptides and SM-102 lipid, DSPE, DMG-PEG_{2000}, and cholesterol (the lipid molar ratio is 50: 10: 1.5: 38.5) was mixed with an aqueous phase of CpG or Svg3 in 10 mM citrate buffer at a flow rate of 2 mL/min. PROTAV LNPs were dialyzed in 1x PBS at 4 ºC for 12 hours using a microdialysis cassette (20,000 MWCO, Thermo Fisher Scientific, Waltham, MA). The diameters and polydispersity index (PDI) of the LNPs were measured with a Zetasizer Nano (Malvern Instruments, Malvern, U.K.).

Cryo-EM of LNPs

LNPs were subject to dialysis and concentration to ~90 mg/mL of lipid using Amicon ultracentrifugation filters. Grids for cryo-EM imaging of samples E7-LNPs, TgT-LNPs, and LNPs were prepared by applying 6 µL purified encapsuling sample at a concentration of 10 mg/ml to a glow-discharged (1 min at 5 mA) Ultrathin Carbon on Quantifoil (R1.2/1.3, 300 mesh, Cu) (Ted Pella, Redding, CA). This was followed by plunge-freezing in liquid ethane using an FEI Vitribot (100% humidity, temperature: 4°C) in two steps: 1) with blot force of 0, wait time of 10 s, and 2) with blot force of 0, wait time of 0 s. Grids were clipped and stored in liquid nitrogen until data collection. Cryo-EM images were collected at the University of Michigan Cryo-EM Facility on a Talos Arctica

transmission electron microscope (Thermo Fisher Scientific, Waltham, MA) with K2 Summit direct detector (Gatan, Pleasanton, CA) operating at 200 kV.

Cell culture

All cells were cultured in medium (Gibco, Brooklyn, NY) supplemented with 10% heat-inactivated FBS, 100 U/mL penicillin, and 100 μg/mL streptomycin, at 37 °C with 5% CO_2. EG7.OVA cells were cultured in RPMI-1640 medium additionally supplemented with 2 mM L-glutamine and 0.4 mg/mL G418. BMDCs, OT-1 cells, DC2.4, and TC-1 cells were cultured in RPMI-1640 medium additionally supplemented with 2 mM l-glutamine, 50 μM 2-mercaptoethanol, 1× non-essential amino acids and 10 mM HEPES. B16F10 cells were cultured in DMEM medium.

BMDC isolation and culture

BMDCs were obtained from 6–8 week old C57BL/6 mice. Femurs and tibias were harvested and cut at the epiphyses, and their bone marrow was flushed out three times with 10 mL RPMI-1640 medium (Gibco, Brooklyn, NY). Cell suspensions were filtered through 70-μm cell strainers (BD Falcon, Franklin Lakes, NJ), centrifuged, and treated with ACK buffer (Gibco, Brooklyn, NY) for lysis. Cell pellets were resuspended in RPMI-1640 medium (10% FBS and 20 ng/mL GM-CSF) to achieve a density of 2×10^6 viable cells per 75-mm petri dish. On day 6, non-adherent and loosely adherent cells were collected as BMDCs by gently washing with PBS and pooled for further studies.

Flow cytometry

Immunostained cultured cells, mouse blood cells, and single-cell suspensions from tumor tissue and lymph node homogenates were analyzed by flow cytometry (Cytek Aurora, Cytek Biosciences, Fremont, CA). The antibodies used for immunostaining are detailed in **Supplementary Table 4**. Data were analyzed using FlowJo V10 software, and representative gating strategies for flow cytometry data analysis are shown in **Supplementary Fig. 17-20**.

***In vitro* and *in vivo* antigen SIINFEKL presentation on DCs**

For in vitro cell study, 2×10^5 DCs were seeded in 24-well plates and treated with PROTAV-OVA, OVA, and controls, respectively, for 24 hours. Harvested DCs were then stained with an APC-labeled anti-mouse H-$2K^b$/SIINFEKL complex antibody (Biolegend). For in vivo studies, C57BL/6 mice were s.c. administered with PROTAV-OVA or OVA (10 μg), and PBS, respectively, with CpG (2 nmole) (Integrated DNA Technologies, Coralville, IW) as adjuvant. After a series of time, draining inguinal lymph nodes were harvested and homogenated to prepare single cells. H-$2K^b$/SIINFEKL complex on DCs was stained as above in the resulting single cells. Cells were analyzed using flow cytometry.

OT-1 $CD8^+$ T cell activation

OT-1 cells were isolated from OT-1 mice (Jackson Laboratory) using $CD8^+$ T cell isolation kit (Miltenyi, Auburn, CA). OT-1 cells were then stained with an intracellular dye CSFE, followed by washing to remove free CSFE dyes. DCs were treated with PROTAV-OVA, OVA, or controls. Next, CSFE-stained OT-1 cells and as-treated DCs with a ratio of 20:1 were co-cultured for up to three days. Upon recognition of SIINFEKL antigen presented on DCs, SIINFEKL-specific OT-1 cells would be activated and proliferate. The OT-1 cell activation can be measured via the CSFE fluorescence signal dilution by flow cytometry.

Intracellular delivery of PROTAV

In vitro intracellular delivery of PROTAV was studied using dye-labeled PROTAV-OVA by confocal microscopy and flow cytometry. PROTAV-OVA was labeled with FITC using NHS-FITC and PROTAV-OVA that was synthesized by maleimide-thiol conjugation of OVA and pomalidomide-EG_4. FITC-PROTAV-OVA and FITC-OVA, respectively, were incubated with DC2.4 cells for up to 24 h, prior to staining with Lysotracker Green DND-26 (Life Technologies, Carlsbad, CA) and Hoechst 33342 (Life Technologies, Carlsbad, CA) according to manufacturers' instructions. Cells were then washed before confocal microscopy (LSM 780, Zeiss, Chesterfield, VA). Cells treated as above were also analyzed by flow cytometric analysis to measure the FITC fluorescence intensity of cells.

RNA-seq

Total RNA extraction was achieved using the AllPrep DNA/RNA Mini Kit (QIAGEN) and included in-column DNase I digestion to ensure the RNA was free of DNA contamination. The extracted RNA's integrity was checked with the Agilent RNA 6000 Pico Kit (Agilent). For mRNA-seq library preparation, 1 µg of total RNA (with an RIN score above 8) was used, according to Illumina stranded mRNA-seq preparation Guide. In brief, total RNA was processed to isolate mRNA using oligo (dT) magnetic beads, which then underwent cation fragmentation and reverse transcription into complementary DNA (cDNA). The cDNA was end-repaired, ligated to RNA index anchors, and PCR-amplified with random primers to generate indexed libraries, using IDT for Illumina UD indexes. After ensuring the quality, these barcoded libraries were equally pooled and paired-end sequenced (2 x 150 bp) on the NextSeq 2000 instrument (Illumina). FastQC v0.11.9 was used to evaluate the quality of RNA-Seq reads. The STAR aligner version 2.7.6a[71] was employed to align reads from individual samples to the mouse reference genome GRCm39. FeatureCounts[72] was used to aggregate raw gene counts of the aligned reads. Differential gene expression analysis was conducted using the Bioconductor package DESeq2 v1.30.0[73] with normalized and filtered gene counts from the RNA-Seq data. Genes exhibiting differential expression with an adjusted p value of less than 0.05 were further analyzed for Gene Ontology and KEGG pathway enrichment analyses using the ORA.

Animal studies

All animal studies were conducted in compliance with the Guide for the Care and Use of Animals under protocols approved by the Institutional Animal Care & Use Committee (IACUC) at University of Michigan and Virginia Commonwealth University.

PBMC T cell responses

Tetramer staining, immune memory, and immune checkpoint expression levels on T cells. Peripheral blood was drawn from vaccinated mice. ACK lysis buffer was used to lyse red blood cells for 10 minutes at room temperature. Any blood clots were filtered out, and the cells were washed twice with PBS. Zombie Aqua™ Fixable Viability Kit (BioLegend, San Diego, CA) was used for live-dead cell staining for 20 minutes at room temperature, followed by cell washing with FCS buffer (PBS with 0.1% FBS). Cells were blocked with αCD16/CD32 (BioLegend, San Diego, CA) for 10 min, and were then incubated with a staining cocktail containing PerCP/Cy5.5 anti-mouse CD3, APC/Cy7 anti-mouse CD8α, CD44--AF647, CD62L-FITC, BV421 anti-mouse PD-1, BV605 anti-mouse Tim-3, and PE-conjugated tetramers (NIH Tetramer Core Facility). After 30 minutes at room temperature, cells were washed, and then fixed using 100 µL Cytofix per each well of 96-well plates at 4°C for 20 minutes. Finally, cells were washed and resuspended with Perm/Wash buffer for analysis by flow cytometry. For immune memory analysis, cells were gated based on $CD44^{high}CD62L^{high}$ $CD8^{+}$ Tcm cells, $CD44^{high}CD62L^{low}$ $CD8^{+}$ Tem cells, and $CD44^{low\text{-}med}CD62L^{high}$ naive $CD8^{+}$ T cells.

Intracellular cytokine staining of T cells. Intracellular cytokine staining in T cells was performed as before.[74] Briefly, peripheral blood from immunized mice was collected and processed as above to obtain lymphocytes and lyse red blood cells. The lymphocytes were then transferred into U-bottom 96-well plates containing 200 µL of T cell culture medium. Cells were restimulated by 40 µg/mL antigen peptides for 4 hours (CS Bio, Menlo Park, CA; peptide sequences in **Supplementary Table 3**), after which GolgiPlug Protein Transport Inhibitor with brefeldin A (Thermo Fisher Scientific) was added. The cells were then incubated for 6 hours prior to αCD16/CD32 staining at room temperature for 10 minutes. Following this, cells were stained with APC/Cy7 anti-mouse CD8α, PerCP/Cy5.5 anti-mouse CD4, and the Zombie Aqua™ Fixable Viability Kit (BioLegend, San Diego, CA) (for 20 minutes at room temperature). Cells were then washed and fixed using Cytofix (BD Biosciences), and were permeabilized with 200 µL Cytoperm solution (BD Biosciences), followed by washing with Perm/Wash Buffer (BD Biosciences). Upon permeabilization, cells were stained with PE anti-mouse IFN-γ and FITC anti-mouse TNF-α (BioLegend). After final washing, the cells were prepared for flow cytometric analysis.

Immune analysis of TME, spleen, and lymph nodes in tumor-bearing mice

Tumors were established by *s.c.* injection of tumor cells at mouse shoulders. Tumor-bearing mice were treated with PROTAV or control vaccines, alone or in combination with ICIs. Blood and tissues of interest were collected four days after the last treatment. Tissues were weighed and dissected into small pieces prior to digestion treatment in RPMI 1640 media (15 min, 37 °C) supplemented with collagenase (Sigma, St Louis, MO) and DNase I (New England Biolabs, Ipswich, MA). Tissues were filtered through a 70 µm cell strainer (Fisher Scientific,

Pittsburg, PA) and treated with ACK Lysing Buffer (Gibco, Brooklyn, NY) for red blood cell lysis. The resulting single cells were then washed and stained with live-dead staining dye, followed by staining with antibody cocktails and tetramers according to the manufacturer's instructions. At the end of staining, cells were washed and fixed prior to flow cytometric analysis as described above.

Tumor immunotherapy

Female C57BL/6 mice (6–8 weeks old, Charles River Laboratories, $n = 6–10$) were *s.c.* injected on the shoulder with 3×10^5 tumor cells (e.g., TC-1, B16F10). Tumor progression was assessed using caliper measurements. Mice were treated when tumor reached a certain volume (e.g., 50 or 300 mm^3). Vaccines were administered subcutaneously at the base of the tail for optimal lymphatic drainage (10-50 µg antigen, 2 nmole CpG and/or 1 nmole Svg3, and 100 µg αPD-1 or αCTLA-4 (Bio X Cell, Inc., NH). αPD-1 or αCTLA-4 was *i.p.* administered. Tumor dimensions and mouse weights were recorded every 3 days. Mice were euthanized if the largest tumor dimension reached 2 cm, tumor volume surpassed 2000 mm^3, or ulceration occurred. Tumor volumes were calculated as (length x $width^2$)/2 and analyzed as previously described, and results were processed using GraphPad Prism 7 (La Jolla, CA).

Statistical analysis

Data represent mean ± s.e.m., unless denoted otherwise. Statistical analysis was performed in GraphPad Prism Software version 5.0. *P*-values were calculated by one-way ANOVA with Bonferroni post-test, unless denoted otherwise.

Reporting Summary

Further information on research design is available in the Nature Research Reporting Summary linked to this article.

Data availability

The data supporting the results in this study are available within the paper and its Supplementary Information. Source data for the figures will be provided with this paper.

References

1. Waldman, A. D., Fritz, J. M. & Lenardo, M. J. A guide to cancer immunotherapy: from T cell basic science to clinical practice. *Nat. Rev. Immunol.* **20**, 651–668 (2020).
2. Mountzios, G. *et al.* Immune-checkpoint inhibition for resectable non-small-cell lung cancer — opportunities and challenges. *Nat. Rev. Clin. Oncol.* **20**, 664–677 (2023).
3. Wolchok, J. D. *et al.* Nivolumab plus ipilimumab in advanced melanoma. *N. Engl. J. Med.* **369**, 122–133 (2013).
4. Tawbi, H. A. *et al.* Combined Nivolumab and Ipilimumab in Melanoma Metastatic to the Brain. *N. Engl. J. Med.* **379**, 722–730 (2018).
5. Nivolumab and Ipilimumab in Melanoma Metastatic to the Brain. *N. Engl. J. Med.* **379**, 2177–2178 (2018).
6. Hu, Z., Ott, P. A. & Wu, C. J. Towards personalized, tumor-specific, therapeutic vaccines for cancer. *Nat. Rev. Immunol.* **18**, 168–182 (2018).
7. Katsikis, P. D., Ishii, K. J. & Schliehe, C. Challenges in developing personalized neoantigen cancer vaccines. *Nat. Rev. Immunol.* **24**, 213–227 (2024).
8. Liu, J. *et al.* Cancer vaccines as promising immuno-therapeutics: platforms and current progress. *J. Hematol. Oncol.J Hematol Oncol* **15**, 28 (2022).
9. Lee, M. Y., Jeon, J. W., Sievers, C. & Allen, C. T. Antigen processing and presentation in cancer immunotherapy. *J. Immunother. Cancer* **8**, e001111 (2020).
10. Blum, J. S., Wearsch, P. A. & Cresswell, P. Pathways of Antigen Processing. *Annu. Rev. Immunol.* **31**, 443–473 (2013).
11. Huang, L., Marvin, J. M., Tatsis, N. & Eisenlohr, L. C. Cutting Edge: Selective Role of Ubiquitin in MHC Class I Antigen Presentation. *J. Immunol.* **186**, 1904–1908 (2011).
12. Wieczorek, M. *et al.* Major Histocompatibility Complex (MHC) Class I and MHC Class II Proteins: Conformational Plasticity in Antigen Presentation. *Front. Immunol.* **8**, (2017).
13. Bai, L. *et al.* A Potent and Selective Small-Molecule Degrader of STAT3 Achieves Complete Tumor Regression In Vivo. *Cancer Cell* **36**, 498-511.e17 (2019).
14. Kaneshige, A. *et al.* A selective small-molecule STAT5 PROTAC degrader capable of achieving tumor regression in vivo. *Nat. Chem. Biol.* **19**, 703–711 (2023).
15. Békés, M., Langley, D. R. & Crews, C. M. PROTAC targeted protein degraders: the past is prologue. *Nat. Rev. Drug Discov.* **21**, 181–200 (2022).
16. Li, R. *et al.* Proteolysis-Targeting Chimeras (PROTACs) in Cancer Therapy: Present and Future. *Molecules* **27**, 8828 (2022).
17. Morreale, F. E. & Walden, H. Types of Ubiquitin Ligases. *Cell* **165**, 248-248.e1 (2016).
18. Li, K. & Crews, C. M. PROTACs: past, present and future. *Chem. Soc. Rev.* **51**, 5214–5236 (2022).
19. Si, L. *et al.* Generation of a live attenuated influenza A vaccine by proteolysis targeting. *Nat. Biotechnol.* **40**, 1370–1377 (2022).
20. Massafra, V. *et al.* Proteolysis-Targeting Chimeras Enhance T Cell Bispecific Antibody-Driven T Cell Activation and Effector Function through Increased MHC Class I Antigen Presentation in Cancer Cells. *J. Immunol.* **207**, 493–504 (2021).
21. Zhou, S. *et al.* Engineering cGAS-agonistic oligonucleotides as therapeutics for cancer immunotherapy. *Mol. Ther. - Nucleic Acids* **35**, (2024).

22. Sester, D. P. *et al.* CpG DNA activates survival in murine macrophages through TLR9 and the phosphatidylinositol 3-kinase-Akt pathway. *J Immunol* **177**, 4473–4480 (2006).
23. Lee, J. *et al.* Discovery of E3 Ligase Ligands for Target Protein Degradation. *Molecules* **27**, 6515 (2022).
24. Garber, K. The PROTAC gold rush. *Nat. Biotechnol.* **40**, 12–16 (2022).
25. Singh, H. & Agrawal, D. K. Recent Advancements in the Discovery of Cereblon-Based Protease-Targeted Chimeras With Potential for Therapeutic Intervention. *Future Med. Chem.* **14**, 1403–1416 (2022).
26. Lu, J. *et al.* Hijacking the E3 Ubiquitin Ligase Cereblon to Efficiently Target BRD4. *Chem. Biol.* **22**, 755–763 (2015).
27. Cieślak, M. & Słowianek, M. Cereblon-Recruiting PROTACs: Will New Drugs Have to Face Old Challenges? *Pharmaceutics* **15**, (2023).
28. Almodóvar-Rivera, C. M. *et al.* A Modular Chemistry Platform for the Development of a Cereblon E3 Ligase-Based Partial PROTAC Library. *Chembiochem* **24**, e202300482.
29. Liu, Y. *et al.* Expanding PROTACtable genome universe of E3 ligases. *Nat. Commun.* **14**, 6509 (2023).
30. Lipford, G. B., Hoffman, M., Wagner, H. & Heeg, K. Primary in vivo responses to ovalbumin. Probing the predictive value of the Kb binding motif. *J. Immunol.* **150**, 1212–1222 (1993).
31. Lu, J., Jiang, F., Lu, A. & Zhang, G. Linkers Having a Crucial Role in Antibody–Drug Conjugates. *Int. J. Mol. Sci.* **17**, 561 (2016).
32. Troup, R. I., Fallan, C. & Baud, M. G. J. Current strategies for the design of PROTAC linkers: a critical review. *Explor. Target. Anti-Tumor Ther.* **1**, 273–312 (2020).
33. Fischer, E. S. *et al.* Structure of the DDB1–CRBN E3 ubiquitin ligase in complex with thalidomide. *Nature* **512**, 49–53 (2014).
34. Cui, C. *et al.* A lysosome-targeted DNA nanodevice selectively targets macrophages to attenuate tumors. *Nat. Nanotechnol.* **16**, 1394–1402 (2021).
35. Fan, W. *et al.* Proteasome inhibitor MG-132 induces C6 glioma cell apoptosis via oxidative stress. *Acta Pharmacol. Sin.* **32**, 619–625 (2011).
36. Lawrence, M. S. *et al.* Mutational heterogeneity in cancer and the search for new cancer-associated genes. *Nature* **499**, 214–218 (2013).
37. Lee, C.-H., Yelensky, R., Jooss, K. & Chan, T. A. Update on Tumor Neoantigens and Their Utility: Why It Is Good to Be Different. *Trends Immunol.* **39**, 536–548 (2018).
38. Roden, R. B. S. & Stern, P. L. Opportunities and challenges for human papillomavirus vaccination in cancer. *Nat. Rev. Cancer* **18**, 240–254 (2018).
39. Peng, S. *et al.* Development of DNA Vaccine Targeting E6 and E7 Proteins of Human Papillomavirus 16 (HPV16) and HPV18 for Immunotherapy in Combination with Recombinant Vaccinia Boost and PD-1 Antibody. *mBio* **12**, (2021).
40. Rumfield, C. S., Pellom, S. T., Ii, Y. M. M., Schlom, J. & Jochems, C. Immunomodulation to enhance the efficacy of an HPV therapeutic vaccine. *J. Immunother. Cancer* **8**, e000612 (2020).
41. Peng, S. *et al.* Development of a DNA Vaccine Targeting Human Papillomavirus Type 16 Oncoprotein E6. *J. Virol.* **78**, 8468–8476 (2004).
42. Karimi, H., Soleimanjahi, H., Abdoli, A. & Banijamali, R. S. Combination therapy using human papillomavirus L1/E6/E7 genes and archaeosome: a nanovaccine confer immuneadjuvanting effects to fight cervical cancer. *Sci. Rep.* **10**, 5787 (2020).

43. Holzinger, D. *et al.* Sensitivity and specificity of antibodies against HPV16 E6 and other early proteins for the detection of HPV16-driven oropharyngeal squamous cell carcinoma. *Int. J. Cancer* **140**, 2748–2757 (2017).
44. Pal, A. & Kundu, R. Human Papillomavirus E6 and E7: The Cervical Cancer Hallmarks and Targets for Therapy. *Front. Microbiol.* **10**, (2020).
45. Nagarsheth, N. B. *et al.* TCR-engineered T cells targeting E7 for patients with metastatic HPV-associated epithelial cancers. *Nat. Med.* **27**, 419–425 (2021).
46. Wang, T.-L. *et al.* Intramuscular administration of E7-transfected dendritic cells generates the most potent E7-specific anti-tumor immunity. *Gene Ther.* **7**, 726–733 (2000).
47. Cid-Arregui, A., Juárez, V. & Hausen, H. zur. A Synthetic E7 Gene of Human Papillomavirus Type 16 That Yields Enhanced Expression of the Protein in Mammalian Cells and Is Useful for DNA Immunization Studies. *J. Virol.* **77**, 4928–4937 (2003).
48. Ji, H. *et al.* Antigen-specific immunotherapy for murine lung metastatic tumors expressing human papillomavirus type 16 E7 oncoprotein. *Int. J. Cancer* **78**, 41–45 (1998).
49. Nagarsheth, N. B. *et al.* TCR-engineered T cells targeting E7 for patients with metastatic HPV-associated epithelial cancers. *Nat. Med.* **27**, 419–425 (2021).
50. Abramson, J. *et al.* Accurate structure prediction of biomolecular interactions with AlphaFold 3. *Nature* **630**, 493–500 (2024).
51. Hodi, F. S. *et al.* Improved survival with ipilimumab in patients with metastatic melanoma. *N. Engl. J. Med.* **363**, 711–723 (2010).
52. Herbst, R. S. *et al.* Predictive correlates of response to the anti-PD-L1 antibody MPDL3280A in cancer patients. *Nature* **515**, 563–567 (2014).
53. Bedard, P. L., Hansen, A. R., Ratain, M. J. & Siu, L. L. Tumor heterogeneity in the clinic. *Nature* **501**, 355–64 (2013).
54. Hu, Z., Ott, P. A. & Wu, C. J. Towards personalized, tumor-specific, therapeutic vaccines for cancer. *Nat. Rev. Immunol.* **18**, 168–182 (2018).
55. van der Burg, S. H., Arens, R., Ossendorp, F., van Hall, T. & Melief, C. J. M. Vaccines for established cancer: overcoming the challenges posed by immune evasion. *Nat. Rev. Cancer* **16**, 219–233 (2016).
56. Sahin, U. & Türeci, Ö. Personalized vaccines for cancer immunotherapy. *Science* **359**, 1355–1360 (2018).
57. Schlom, J. & Gulley, J. L. Vaccines as an Integral Component of Cancer Immunotherapy. *JAMA* **320**, 2195–2196 (2018).
58. Melero, I. *et al.* Evolving synergistic combinations of targeted immunotherapies to combat cancer. *Nat. Rev. Cancer* **15**, 457–472 (2015).
59. Guevara-Patiño, J. A. *et al.* Optimization of a self antigen for presentation of multiple epitopes in cancer immunity. *J. Clin. Invest.* **116**, 1382–1390 (2006).
60. Muranski, P. *et al.* Tumor-specific Th17-polarized cells eradicate large established melanoma. *Blood* **112**, 362–373 (2008).
61. Muranski, P. *et al.* Treatment of Established B16 Murine Melanoma Tumors with Tyrp-1 Specific CD4+ Lymphocytes. *Blood* **108**, 3688–3688 (2006).
62. Leitner, W. W. *et al.* Alphavirus-based DNA vaccine breaks immunological tolerance by activating innate antiviral pathways. *Nat. Med.* **9**, 33–39 (2003).

63. Rosalia, R. A. *et al.* Dendritic cells process synthetic long peptides better than whole protein, improving antigen presentation and T-cell activation. *Eur. J. Immunol.* **43**, 2554–2565 (2013).
64. Lee, C.-H., Yelensky, R., Jooss, K. & Chan, T. A. Update on Tumor Neoantigens and Their Utility: Why It Is Good to Be Different. *Trends Immunol.* **39**, 536–548 (2018).
65. Binnewies, M. *et al.* Understanding the tumor immune microenvironment (TIME) for effective therapy. *Nat. Med.* **24**, 541 (2018).
66. Usset, J. *et al.* Five latent factors underlie response to immunotherapy. *Nat. Genet.* 1–9 (2024) doi:10.1038/s41588-024-01899-0.
67. Noren, C. J., Anthony-Cahill, S. J., Griffith, M. C. & Schultz, P. G. A General Method for Site-specific Incorporation of Unnatural Amino Acids into Proteins. *Science* **244**, 182–8 (1989).
68. Shi, N. *et al.* Restoration of dystrophin expression in mice by suppressing a nonsense mutation through the incorporation of unnatural amino acids. *Nat. Biomed. Eng.* **6**, 195–206 (2022).
69. Alameh, M.-G. *et al.* Lipid nanoparticles enhance the efficacy of mRNA and protein subunit vaccines by inducing robust T follicular helper cell and humoral responses. *Immunity* **54**, 2877-2892.e7 (2021).
70. Yang, T. *et al.* Conjugation of glucosylated polymer chains to checkpoint blockade antibodies augments their efficacy and specificity for glioblastoma. *Nat. Biomed. Eng.* **5**, 1274–1287 (2021).
71. Dobin, A. *et al.* STAR: ultrafast universal RNA-seq aligner. *Bioinformatics* **29**, 15–21 (2013).
72. Liao, Y., Smyth, G. K. & Shi, W. featureCounts: an efficient general purpose program for assigning sequence reads to genomic features. *Bioinformatics* **30**, 923–930 (2014).
73. Love, M. I., Huber, W. & Anders, S. Moderated estimation of fold change and dispersion for RNA-seq data with DESeq2. *Genome Biol.* **15**, 550 (2014).
74. Zhu, G. *et al.* Albumin/vaccine nanocomplexes that assemble in vivo for combination cancer immunotherapy. *Nat. Commun.* **8**, 1954 (2017).

Acknowledgements

G.Z. acknowledges funding support from NIH (R01CA286122, R01CA266981, R01AI168684, R35GM143014), DoD CDMRP Breast Cancer Breakthrough Award Level II (BC210931/P1), American Cancer Society Research Scholar Grant (RSG-22-055-01-IBCD), University of Michigan Rogel Cancer Center Discovery Award. Research reported in this publication was supported by the National Cancer Institute under Award Number P30 CA046592 by the use of the following Cancer Center Shared Resource: Flow Cytometry, Immune Monitoring, Pharmacokinetics, and Proteomics. We thank the University of Michigan ULAM (Unit for Laboratory Animal Medicine) In Vivo Animal Core (IVAC) and the Center for Structural Biology for providing service. We thank the Genomics Core, and Bioinformatics Shared Resource and Flow Cytometry Shared Resource at Massey Comprehensive Cancer Center (MCCC) at Virginia Commonwealth University for providing service. MCCC is supported, in part, with funding from NIH-NCI Cancer Center Support Grant P30 CA016059. We thank NIH Tetramer Core for kindly providing tetramer reagents. The content is solely the responsibility of the authors and does not necessarily represent the official views of the National Institutes of Health.

Author contributions

G.Z., T.S., and F.C. initiated the project. G.Z., T.S., F.C., and Q.W. designed the project. T.S., F.C., Q.W., X.L., S.Z., M.W., Y.X., S.L., J.D., G.X., H.W., W.Z., B.W., V.B. performed experiments. R.T., K.M.T., J.Z. analyzed RNAseq data. G.Z., Q.W., T.S., F.C., D.X., and S.W. analyzed data. G.Z. and Q.W. drafted the manuscript. All authors reviewed the manuscript.

Competing interests

G.Z., T.S., F.C., and Q.W. were listed as inventors in a related patent application. The other authors declare no conflicts of interest.

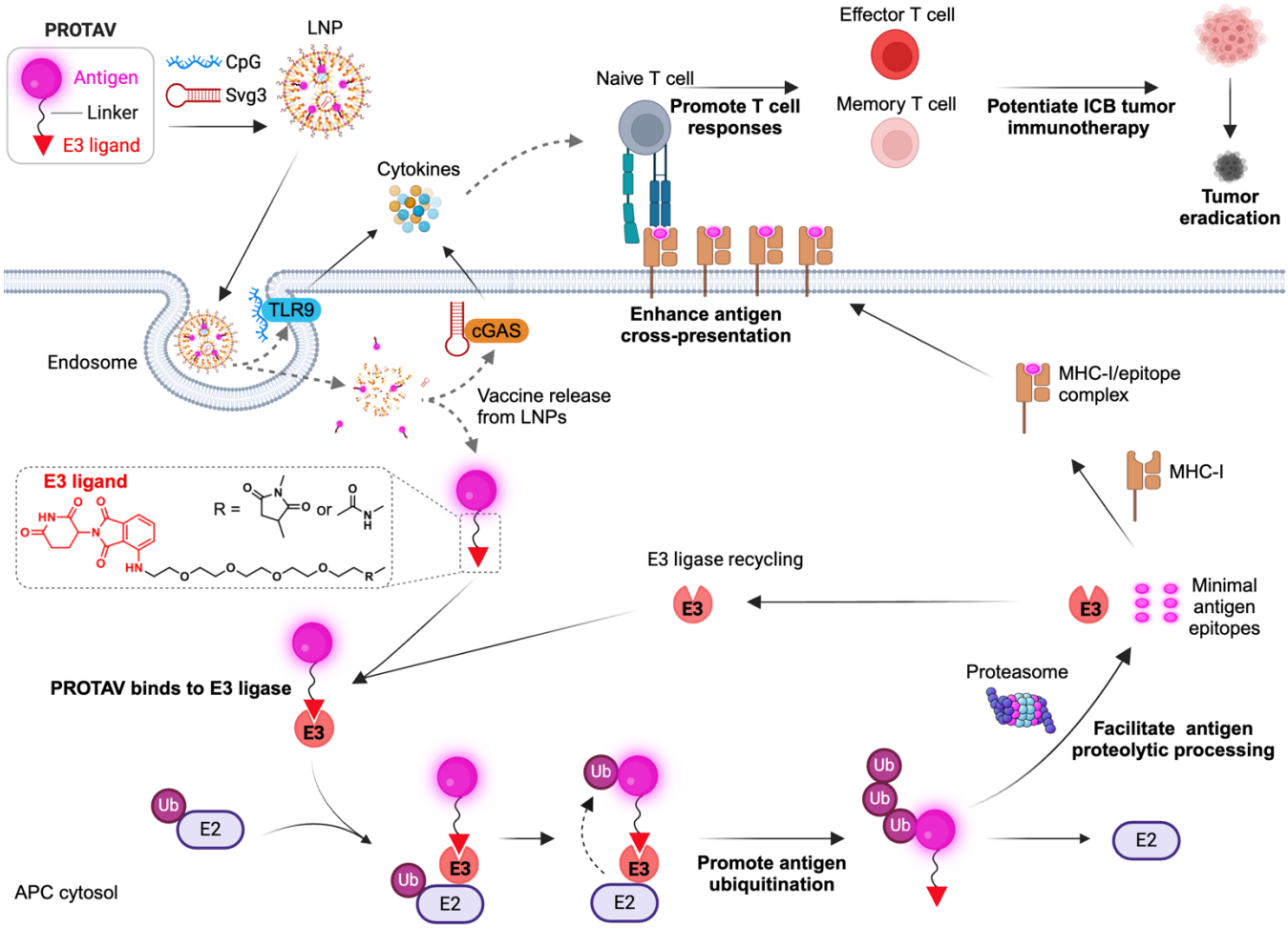

Fig. 1. Schematic illustration of PROTAVs that facilitate antigen proteolytic processing and antigen cross-presentation to potentiate antitumor T cell responses for robust ICB combination immunotherapy of tumor. A PROTAV is a covalent conjugate of a protein/peptide antigen and an E3 ligase-binding ligand, with a chemical linker in between. PROTAVs are broadly applicable for common types of tumor protein/peptide antigens, including proteins, synthetic long peptides, and multivalent fusion peptides. Upon delivery into APCs by LNPs, PROTAVs are bound to endogenous E3 ligases, which promoted the ubiquitination of the antigens in PROTAVs, facilitated antigen proteolytic processing by proteasome, promoted antigen cross-presentation to T cells, thereby potentiating antigen-specific T cell responses. Peptide antigen-based PROTAVs were co-loaded with two oligonucleotide immunostimulant adjuvants, Svg3 and CpG, in LNPs for optimal PROTAV/adjuvant codelivery into APCs. The bi-adjuvants of Svg3 and CpG activate cGAS and TLR9, respectively, to elicit proinflammatory responses, including type-I interferon (IFN) responses. As a result, PROTAVs potentiated antitumor $CD8^+$ cytotoxic T cell responses. The combination of PROTAVs with ICB remodeled the tumor immune microenvironment, facilitated tumor regression, and promoted the CR rates of tumors, including ICB-resistant large tumors. LNP: lipid nanoparticle; cGAS: cyclic GMP-AMP synthase; Svg3: an oligonucleotide agonist for cGAS; TLR9: Toll-like receptor 9; CpG: an oligonucleotide agonist for TLR9; E2: E2 ligase; E3: E3 ligase; Ub: ubiquitin; APC: antigen-presenting cell; MHC: major histocompatibility complex; ICB: immune checkpoint blockade. Created in BioRender.

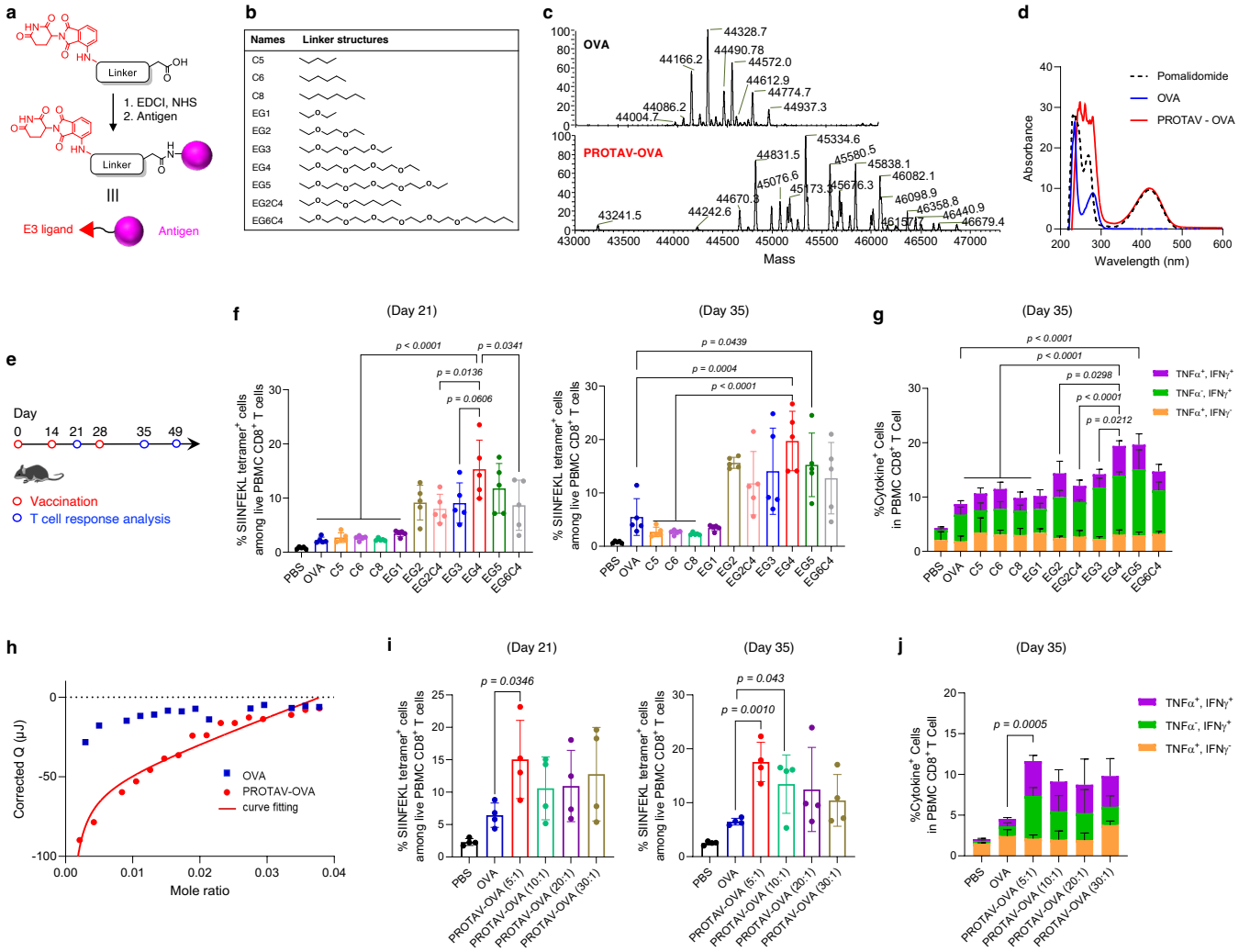

Fig. 2 I Linker optimization for PROTAV-OVA to elicit potent T cell response in mice. **a**, Representative synthesis route for PROTAVs via EDC-NHS conjugation. **b**, The chemical structures of a list of linkers screened for PROTAV-OVA. **c**, Deconvoluted ESI-MS spectra of OVA and PROTAV-OVA with an EG_4 linker. **d**, UV-vis absorbance spectra of pomalidomide, OVA, and PROTAV-OVA (i.e., pomalidomide-OVA conjugates). The presence of pomalidomide-characteristic absorption (peak at 420 nm) in PROTAV-OVA suggests its successful synthesis. **e**, Timeline of T cell response study for PROTAV-OVA in mice. C57BL/6 mice (6-8 weeks; $n = 5$) were immunized with PROTAVs and controls, individually, by *s.c.* administration at tail base (day 0, day 14). CpG (2 nmole) adjuvant was mixed with OVA or PROTAV-OVA (10 μg). PBMCs were collected for T cell response analysis at indicated time points. **f, g**, H-2K^b/SIINFEKL tetramer staining results (day 21, day 35) (**f**) and intracellular cytokine staining (day 35) (**g**) showing the fraction of SIINFEKL-specific T cell response among PBMC CD8$^+$ T cells elicited by PROTAV-OVA candidates with various linkers. PROTAV-OVA with an EG_4 linker consistently elicited one of the most potent T cell responses. **h**, Nano ITC results and fitted curve of the binding kinetics between PROTAV-OVA with CRBN protein, with OVA as a control. K_d of PROTAV-OVA and CRBN binding was determined to be 1.2 μM using a one site-specific binding model. OVA and CRBN ITC data did not fit into the binding modeling, suggesting negligible binding. **i-j**, H-2K^b/SIINFEKL tetramer staining results (day 21, day 35) (**i**) and intracellular cytokine staining (day 35) (**j**) showing the fraction of SIINFEKL-specific T cell response among PBMC CD8$^+$ T cells elicited by PROTAV-OVA synthesized with four different feeding molar ratios of pomalidomide-EG_4-NHS: OVA. Data represent mean ± s.e.m.; statistical analysis was conducted using one-way ANOVA with Bonferroni post-test.

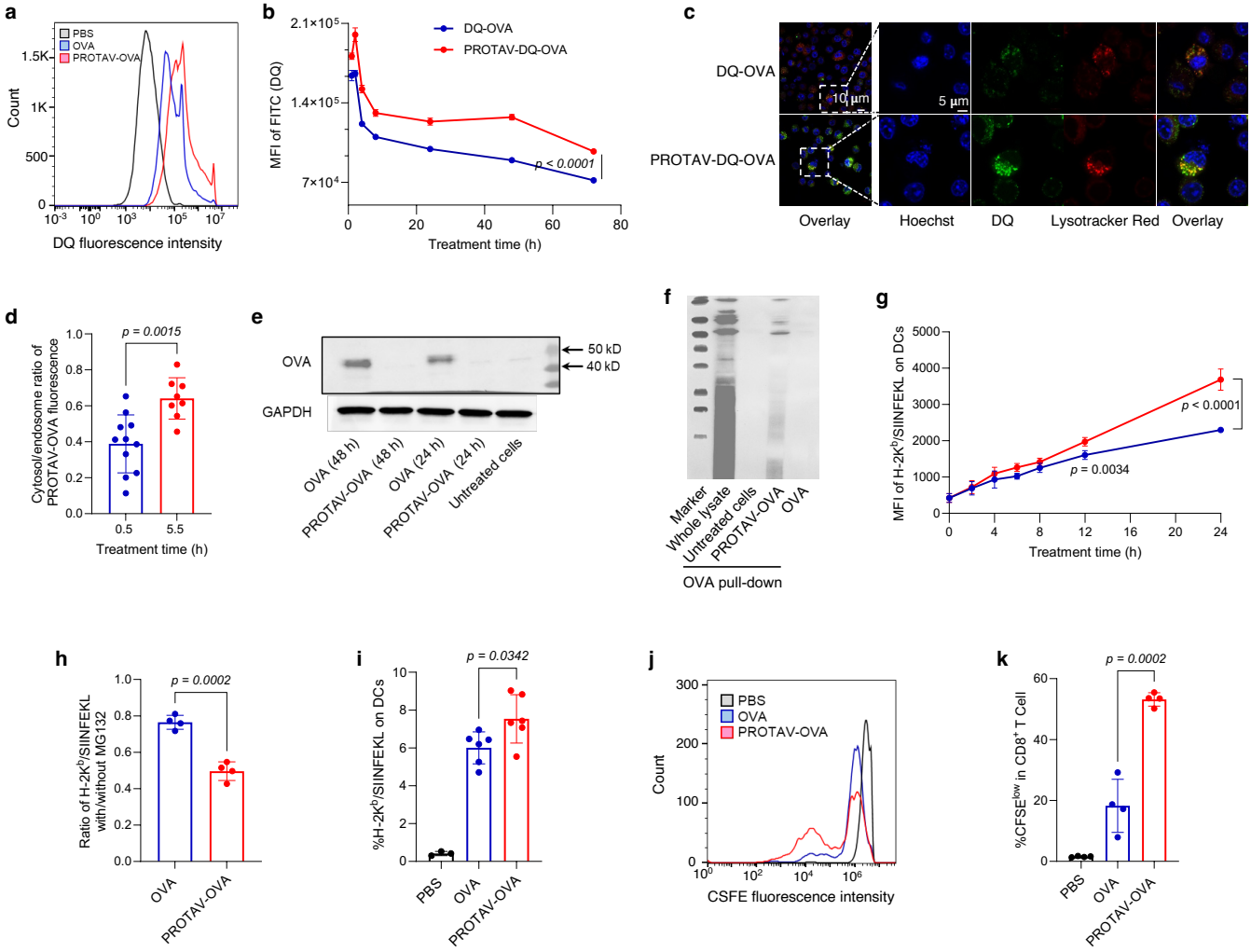

Fig. 3. **PROTAV promoted antigen proteolytic processing and facilitated antigen presentation in DCs *in vitro* and *in vivo*. a-b**, Representative flow cytometry graph (**a**) and MFI quantified from flow cytometry data (**b**) showing that PROTAV-OVA-DQ facilitated OVA-DQ degradation (antigen processing) than OVA-DQ in DCs after a 24-h treatment (**a**) and over the course of 72 h post treatment (**b**). **c**, Confocal microscopy images showing stronger DQ fluorescence recovery of DCs treated with PROTAV-OVA-DQ than cells treated with OVA-DQ (1 h). **d**, The ratios of cytosolic over endolysosomal DQ fluorescence intensities in DCs, after treatment for 0.5 h and 5.5 h, respectively. Cells were treated with PROTAV-OVA-DQ for 0.5 h. One group of cells were subject to imaging, and the other group of cells were washed with cell culture medium to remove extracellular PROTAV-OVA-DQ, followed by another 5-h incubation before imaging. Data were quantified from confocal microscopy images. **e**, A WB image showing that after DCs were treated with PROTAV-OVA and OVA, respectively, PROTAV-OVA resulted in elevated OVA degradation relative to OVA after the corresponding treatment durations (24 h or 48 h). **f**, A co-IP image showing that PROTAV-OVA promoted the ubiquitination of OVA relative to unconjugated OVA in DC2.4 cells after treatment for 12 h. **g**, MFI of H-2K^b/SIINFEKL on DCs quantified from flow cytometry data showing that PROTAV-OVA promoted the presentation of SIINFEKL antigen epitope on DCs over the course of 24-h treatment. H-2K^b/SIINFEKL on DCs was stained using a dye-labeled antibody. **h**, Protease inhibitor MG132 offsets the ability of PROTAV-OVA to facilitate antigen presentation on DCs. In **g-h**, vaccines were transfected into DCs using lipofectamine 2000. **i**, Quantified flow cytometry results showing the percentage of H-2K^b/SIINFEKL-positive DCs among total live DCs from draining inguinal lymph nodes in C57BL/6 mice treated with PROTAV-OVA-DQ or OVA-DQ, respectively. Vaccines were s.c. administered at mouse tail base (dose: 10 μg OVA or PROTAV-OVA, 2 nmole CpG). **j-k**, Representative flow cytometry graphs (**j**) and quantified flow cytometry results showing the CSFE-low OT-1 CD8$^+$ T cells upon co-culture (96 h) with DCs pre-treated (24 h)

with PROTAV-OVA or OVA, respectively. This suggests that relative to OVA, PROTAV-OVA promoted the ability of DCs to expand antigen-specific T cells, as indicated by the CSFE signal dilution of OT-1 cells during cell division. 10 mg/mL PROTAV-OVA or OVA was used in all *in vitro* studies. Data represent mean ± s.e.m.; statistical analysis was conducted by one-way ANOVA with Bonferroni post-test.

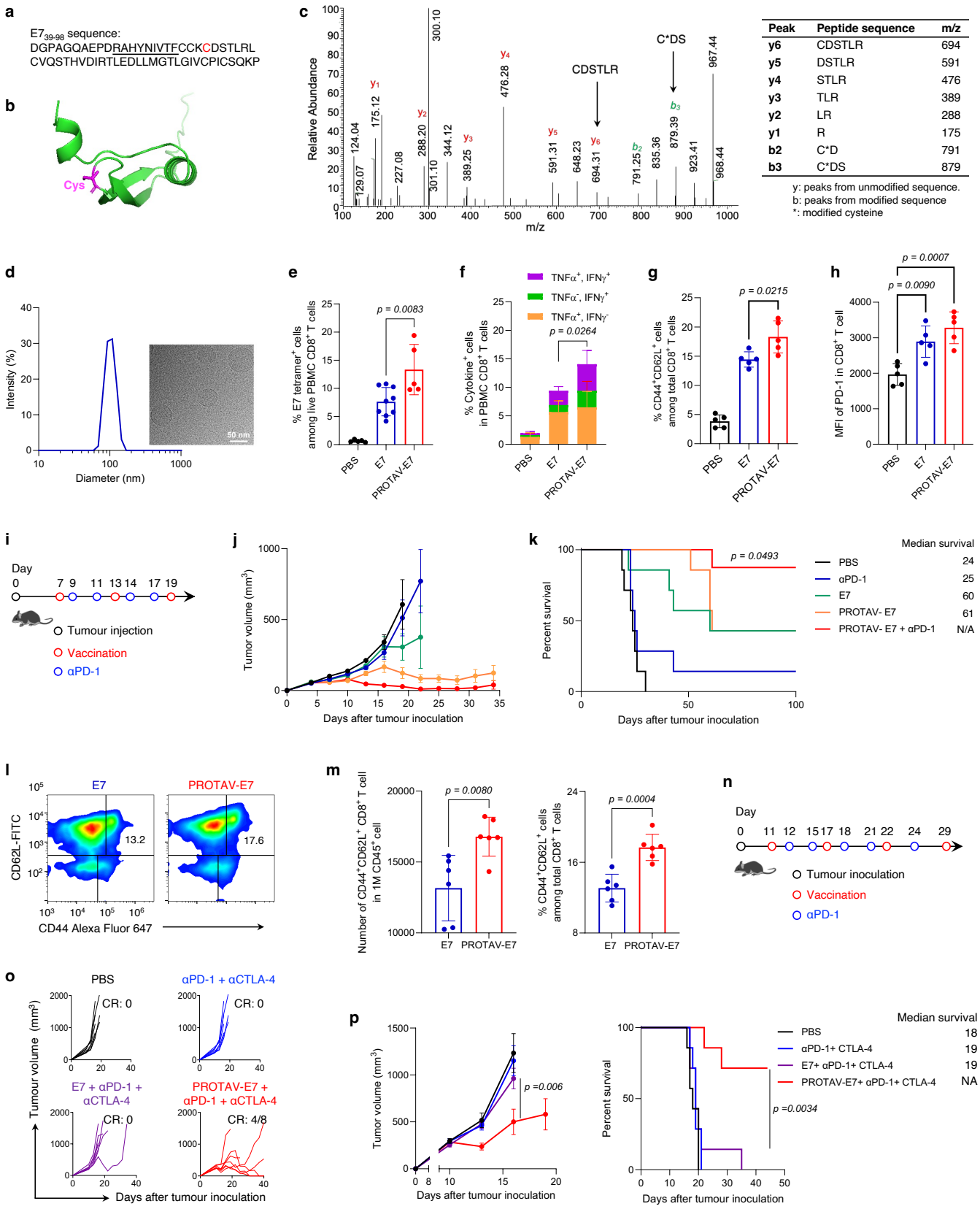

Peak	Peptide sequence	m/z
y6	CDSTLR	694
y5	DSTLR	591
y4	STLR	476
y3	TLR	389
y2	LR	288
y1	R	175
b2	C*D	791
b3	C*DS	879

y: peaks from unmodified sequence.
b: peaks from modified sequence
*: modified cysteine

Fig. 4 I PROTAV-E7 elicited potent E7-specific T cell responses for robust combination immunotherapy of large HPV-associated tumors in mice. a, Sequence of the $E7_{39-98}$ synthetic long peptide used in PROTAV-E7. Underlined: minimal peptide epitope $E7_{49-57}$; red: pomalidomide-EG4-maleimide conjugation site. **b**, Structure of $E7_{39-98}$ predicted by AlphFold3. Cysteines were marked. **c**, LC-Tandem MS results showing the EG_4-pomlidomide conjugation site mapping on $E7_{39-98}$. C61 was identified as a primary site for EG_4-pomlidomide conjugation. **d**, DLS data and a cryo-EM image showing the hydrodynamic sizes and morphology of LNPs co-loaded with PROTAV-E7, CpG, and Svg3. CpG: Svg3 molar ratio: 2:1. Nucleic acid over lipids N:P ratio: 6:1. **e**, H-$2D^b$/$E7_{49-57}$ tetramer staining results showing the percentages of E7-specific $CD8^+$ T cells among total live PBMC $CD8^+$ T cells (day 21) from mice immunized with PROTAV-E7 vaccine or controls (day 0, day 14). Relative to E7, PROTAV-E7 promoted E7-specific $CD8^+$ T cell responses. C57BL/6 mice (6-8 weeks) were immunized with PROTAV-E7 and E7 vaccines, respectively. Vaccines were loaded in SM-102 LNPs (dose: 20 µg antigen, 2 nmole CpG, 1 nmole Svg3) and were *s.c.* injected at mouse tail base. **f**, Intracellular cytokine staining results showing that relative to E7, PROTAV-E7 promoted the fraction of multifunctional cytokine-producing PBMC $CD8^+$ T cells upon antigen restimulation. **g**, Flow cytometry results showing the CD44 and CD62L staining of PBMC $CD8^+$ T cells (day 21) from mice immunized as above, suggesting that PROTAV-E7 elicited great $CD8^+$ T cell memory relative to E7. **h**, MFI of PD-1 on PBMC $CD8^+$ T cells from the above immunized mice. **i**, Timeline of therapy study in small TC-1 tumor (50 mm^3) using PROTAV-E7, alone or combined with αPD-1. Vaccines were loaded in SM-102 LNPs (dose: 20 µg antigen, 2 nmole CpG, 1 nmole Svg3) and were *s.c.* injected at mouse tail base. αPD-1: 100 µg *i.p.* administration. **j**, Tumor grow curves showing that, relative to E7, PROTAV-E7 facilitated the tumor regression and promoted the therapeutic response in E7-positive TC-1 tumor in syngeneic mice. Combining PROTAV-E7 with αPD-1 further promoted the therapeutic efficacy. **k**, Kaplan-Meier mouse survival curves upon the above treatments. **l**, Flow cytometry results showing the cell counts and fractions of $CD8^+$ Tcm cells among total live PBMC $CD8^+$ T cells, 30 days after tumor CR. **n**, Timeline of therapy study in large TC-1 tumor (300 mm^3 at the beginning of treatment) using PROTAV-E7, alone or combined with αPD-1 + αCTLA-4. Vaccines were loaded in SM-102 LNPs (dose: 50 µg antigen, 2 nmole CpG, 1 nmole Svg3) and were *s.c.* injected at mouse tail base. ICB antibodies: 100 µg/each, *i.p.* administration. **o**, Individual tumor growth curves after the indicated treatment. PROTAV-E7 + αPD-1 + αCTLA-4 led to 4/8 tumor CR, in contrast no CR for any other treatments. **p.** Average tumor growth curves (left) and Kaplan-Meier survival curves (right) showing that, relative to E7, PROTAV-E7 promoted the CR rates of large ICI-resistant TC-1 tumors in combination with αPD-1 + αCTLA-4. CR: complete regression. Data represent mean ± s.e.m. (n = 6-8); statistical analysis was conducted by *t*-test (**e-h**) or one-way ANOVA with Bonferroni post-test (**j-p**).

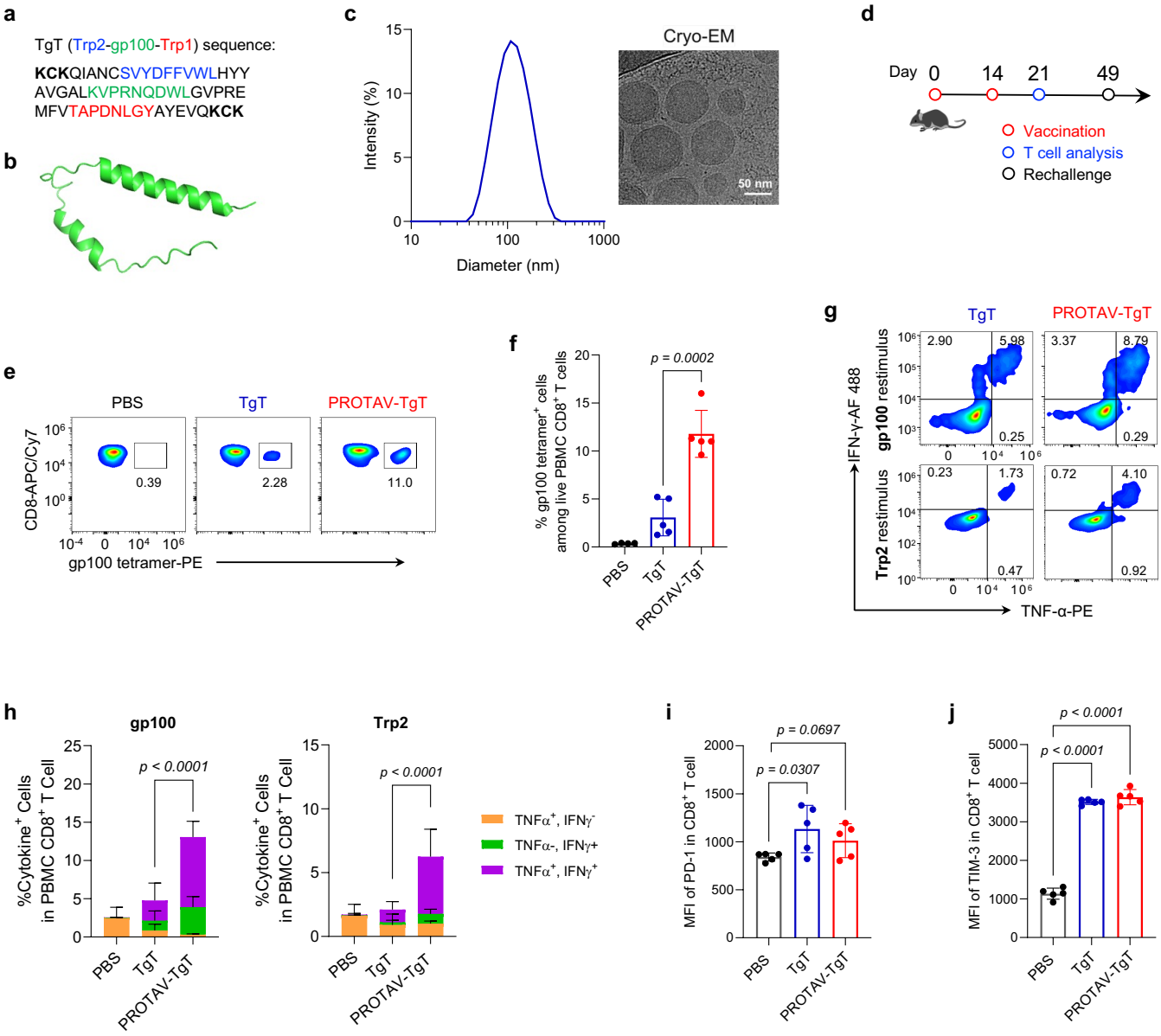

Fig. 5 I Multivalent PROTAV-TgT elicited potent antigen-specific T cell responses. a, Sequence of the TgT multivalent antigenic peptide used in PROTAV-TgT. Minimal peptides were underlined. Multiple terminal K and C were added to promote pomalidomide conjugation via maleimide-thiol conjugation and ubiquitination on lysine, respectively. **b**, Structure of TgT predicted by AlphFold3. **c**, DLS data and a cryo-EM image showing the hydrodynamic sizes and morphology of SM-102 LNPs co-loaded with PROTAV-TgT, CpG, and Svg3. CpG: Svg3 molar ratio: 2: 1. Nucleic acid over lipids N:P ratio: 6:1. **d**, Timeline of PROTAV-TgT immunization study in mice. C57BL/6 mice (6-8 weeks) were immunized with PROTAV-TgT and TgT vaccines, respectively (s.c. at tail base, day 0 and day 14). Dose: 20 ug antigen, 2 nmole CpG, and 1 nmole Svg3. **e-j**, PROTAV-TgT elicited potent multivalent T cell responses while upregulating immune checkpoint levels on T cells in mice. **e-f**, Representative flow cytometry graphs (**e**) and quantified flow cytometry data for tetramer staining results showing that relative to TgT, PROTAV-TgT promoted gp100-specific CD8+ T cell responses (day 21). **g-h**, Representative flow cytometry graphs (**g**) and quantified intracellular cytokine staining results (**h**) of CD8+ T cells upon ex vivo restimulation of PBMC CD8+ T cells with gp100 and Trp2 peptides, respectively, suggesting that relative to TgT, PROTAV-TgT promoted multifunctional T cell responses producing antitumor cytokines. **i-j**, MFI of PD-1 (**i**) and Tim-3 (**j**) on total live PBMC CD8+ T cells in the as-immunized mice, suggesting that PROTAV-TgT upregulated these immune

checkpoint levels on T cells. Data represent mean ± s.e.m. ($n = 5$); statistical analysis was conducted using one-way ANOVA with Bonferroni post-test unless denoted otherwise.

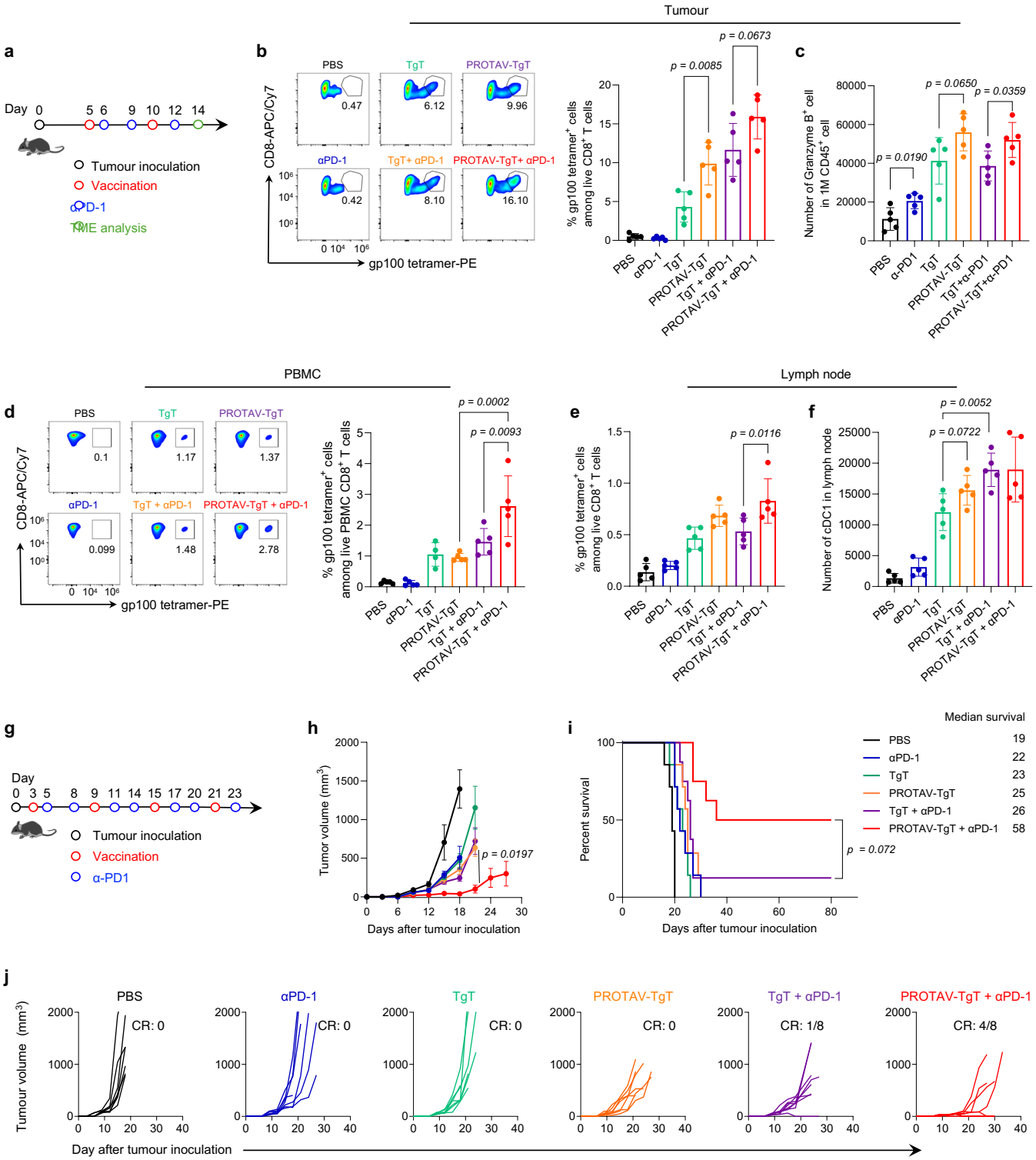

Fig. 6 I PROTAV-TgT, in combination with αPD-1, elicited systemic antitumor immunity and remodeled the tumor immune microenvironment for robust melanoma immunotherapy. a, Timeline for the study of systemic and TME immunomodulation by PROTAV-TgT, alone or combined with αPD-1, in C57BL/6 mice with B16F10 melanoma. **b**, Representative flow cytometry graphs (left) and quantified flow cytometry results (right) of gp100/H-2D^b tetramer staining of intratumoral gp100-specific CD8$^+$ T cells. Relative to TgT, PROTAV-TgT, alone or combined with αPD-1, promoted the tumor infiltration of antitumor CD8$^+$ T cells, as shown by gp100-specific

$CD8^+$ T cells analyzed as an example by tetramer staining. **c**, Flow cytometry results showing the fractions of granzyme B-producing $CD8^+$ T cells among total live $CD8^+$ T cells from as-treated tumors. Relative to TgT + aPD-1, PROTAV-TgT + aPD-1 promoted the fraction of granzyme B-producing $CD8^+$ T cells among total $CD8^+$ T cells in melanoma. **d**, Representative flow cytometry graphs (left) and quantified flow cytometry results (right) of gp100/H-$2D^b$ tetramer staining of PBMC gp100-specific $CD8^+$ T cells from mice treated as above. Relative to TgT, PROTAV-TgT, alone or combined with αPD-1, promoted the fraction of gp100-specific $CD8^+$ T cells among total live PBMC $CD8^+$ T cells. **e**, Quantified flow cytometry results of gp100/H-$2D^b$ tetramer staining showing the fractions of gp100-specific $CD8^+$ T cells among lymph node total live $CD8^+$ T cells. **f**, Quantified flow cytometry results showing the numbers of cDC1 in lymph nodes. Relative to TgT, PROTAV-TgT, alone or combined with αPD-1, promoted the lymph node infiltration of gp100-specific $CD8^+$ T cells (**e**) and cDC1 cells (**f**). **g**, Timeline for melanoma therapy study using PROTAV-TgT, alone or combined with αPD-1. **h-i**, Tumor growth curves (**h**) and Kaplan-Meier mouse survival curves of the above mice (**i**) showing that, relative to TgT, PROTAV-TgT, alone or combined with αPD-1, facilitated the tumor regression, promoted the therapeutic response in B16F10 melanoma, and improved mouse survival in syngeneic mice. **j**, Individual tumor growth curves of B16F10 melanoma treated as above. CR: complete regression. Vaccines: loaded in SM-102 LNPs (dose: 50 µg antigen, 2 nmole CpG, 1 nmole Svg3) and *s.c.* injected at mouse tail base. αPD-1: 100 µg, *i.p.* administration. Data represent mean ± s.e.m. (n = 7-8); statistical analysis was conducted using one-way ANOVA with Bonferroni post-test.